Cell

A β-hydroxybutyrate shunt pathway generates anti-obesity ketone metabolites

Graphical abstract

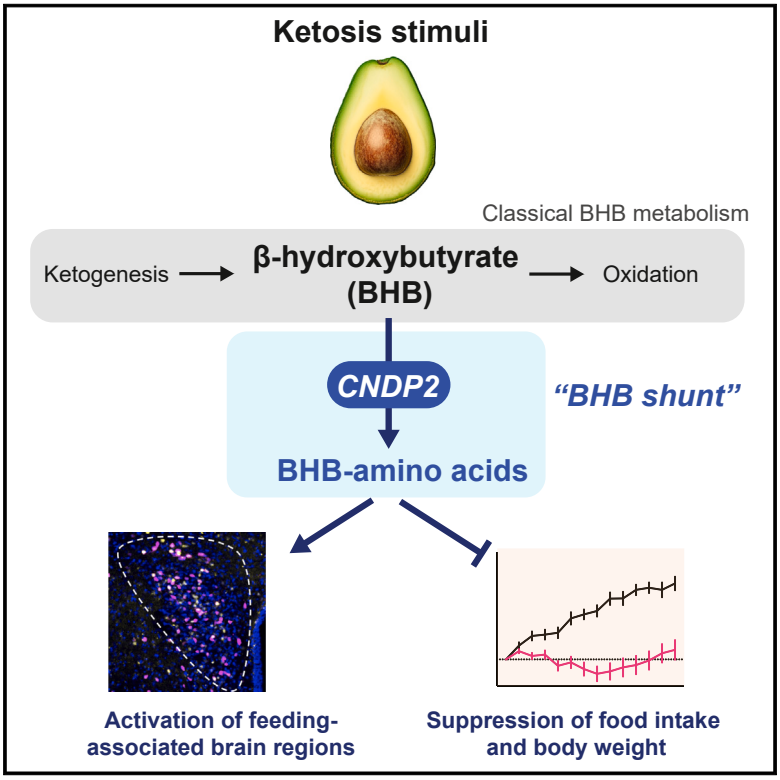

Authors

Maria Dolores Moya-Garzon, Mengjie Wang, Veronica L. Li, ..., Steven M. Banik, Yong Xu, Jonathan Z. Long

Correspondence

yongx@bcm.edu (Y.X.), jzlong@stanford.edu (J.Z.L.)

In brief

Conserved ketone body-amino acid metabolites suppress food intake in mice, demonstrating that secondary ketone body metabolism contributes to energy balance.

Highlights

- A ketone shunt derivatizes β-hydroxybutyrate by conjugation with amino acids
- BHB-amino acids are endogenous mouse and human metabolites
- BHB-Phe administration decreases food intake and body weight in obese mice

Moya-Garzon et al., 2025, Cell *188*, 175–186
January 9, 2025
https://doi.org/10.1016/j.cell.2024.10.032

CellPress

Cell

CellPress
OPEN ACCESS

Article

A β-hydroxybutyrate shunt pathway generates anti-obesity ketone metabolites

Maria Dolores Moya-Garzon,[1,6,8,17] Mengjie Wang,[15,17] Veronica L. Li,[1,2,6,8,17] Xuchao Lyu,[1,6,8] Wei Wei,[1,5,6] Alan Sheng-Hwa Tung,[1,5,6] Steffen H. Raun,[9] Meng Zhao,[1,7,10] Laetitia Coassolo,[1,7,10] Hashim Islam,[11] Barbara Oliveira,[11] Yuqin Dai,[6] Jan Spaas,[1,6] Antonio Delgado-Gonzalez,[3] Kenyi Donoso,[4] Aurora Alvarez-Buylla,[5] Francisco Franco-Montalban,[12] Anudari Letian,[13] Catherine P. Ward,[14] Lichao Liu,[10] Katrin J. Svensson,[1,7,10] Emily L. Goldberg,[13] Christopher D. Gardner,[14] Jonathan P. Little,[11] Steven M. Banik,[2,6] Yong Xu,[15,*] and Jonathan Z. Long[1,6,7,8,16,18,*]

[1]Department of Pathology, Stanford University School of Medicine, Stanford, CA, USA
[2]Department of Chemistry, Stanford University, Stanford, CA, USA
[3]Department of Microbiology and Immunology, Stanford University, Stanford, CA, USA
[4]Department of Urology, Stanford University School of Medicine, Stanford, CA, USA
[5]Department of Biology, Stanford University, Stanford, CA, USA
[6]Sarafan ChEM-H, Stanford University, Stanford, CA, USA
[7]Stanford Diabetes Research Center, Stanford University, Stanford, CA, USA
[8]Wu Tsai Human Performance Alliance, Stanford University, Stanford, CA, USA
[9]Department of Biomedical Sciences, University of Copenhagen, Copenhagen, Denmark
[10]Stanford Cardiovascular Institute, Stanford University School of Medicine, Stanford, CA, USA
[11]School of Health and Exercise Sciences, University of British Columbia, Kelowna, BC, Canada
[12]Departamento de Química Farmacéutica y Orgánica, Universidad de Granada, Campus de Cartuja sn, 18071 Granada, Spain
[13]Department of Physiology, University of California, San Francisco, San Francisco, CA, USA
[14]Stanford Prevention Research Center, Department of Medicine, Stanford University School of Medicine, Stanford, CA, USA
[15]USDA/ARS Children's Nutrition Research Center, Department of Pediatrics, Baylor College of Medicine, Houston, TX, USA
[16]The Phil & Penny Knight Initiative for Brain Resilience at the Wu Tsai Neurosciences Institute, Stanford University, Stanford, CA, USA
[17]These authors contributed equally
[18]Lead contact
*Correspondence: yongx@bcm.edu (Y.X.), jzlong@stanford.edu (J.Z.L.)
https://doi.org/10.1016/j.cell.2024.10.032

SUMMARY

β-Hydroxybutyrate (BHB) is an abundant ketone body. To date, all known pathways of BHB metabolism involve the interconversion of BHB and primary energy intermediates. Here, we identify a previously undescribed BHB secondary metabolic pathway via CNDP2-dependent enzymatic conjugation of BHB and free amino acids. This BHB shunt pathway generates a family of anti-obesity ketone metabolites, the BHB-amino acids. Genetic ablation of CNDP2 in mice eliminates tissue amino acid BHB-ylation activity and reduces BHB-amino acid levels. The most abundant BHB-amino acid, BHB-Phe, is a ketosis-inducible congener of Lac-Phe that activates hypothalamic and brainstem neurons and suppresses feeding. Conversely, CNDP2-KO mice exhibit increased food intake and body weight following exogenous ketone ester supplementation or a ketogenic diet. CNDP2-dependent amino acid BHB-ylation and BHB-amino acid metabolites are also conserved in humans. Therefore, enzymatic amino acid BHB-ylation defines a ketone shunt pathway and bioactive ketone metabolites linked to energy balance.

INTRODUCTION

Mammals have evolved complex nutrient-responsive pathways that link the availability of external energy sources to internal metabolic homeostasis. These pathways involve changes to cellular energy metabolites, which function both as metabolic fuels and as downstream effectors. A key example is the metabolite β-hydroxybutyrate (BHB), a ketone body whose levels rise during periods of low carbohydrate availability, such as during starvation, intermittent fasting, or with consumption of a ketogenic diet.[1,2] BHB is used as a metabolic fuel that can be oxidized by metabolic tissues like the brain and heart for ATP production. In addition, BHB is also a signaling molecule that can activate G-protein-coupled receptors,[3,4] post-translationally modify proteins,[5] or inhibit nuclear histone deacetylases[6] to alter cellular and metabolic processes.

The classical primary metabolic pathways that mediate hepatic BHB production and extrahepatic BHB oxidation

are well established. In hepatic ketogenesis, fatty acid oxidation leads to the production of acetyl-coenzyme A (CoA), which, via the sequential enzymatic action of HMGCS2 (3-hydroxymethylglutaryl-CoA synthase 2), HMGCL (3-hydroxy-3-methylglutaryl-CoA lyase), and BDH1 (3-hydroxybutyrate dehydrogenase 1), ultimately results in generation of BHB.[7] Once produced and exported into the circulation,[8] BHB can then be taken up by extrahepatic tissues, where it undergoes oxidation via BDH1, SCOT (succinyl-CoA:3-ketoacid CoA transferase), and the TCA (tricarboxylic acid) cycle.[9] Importantly, all known metabolic pathways of BHB involve the same metabolic interconversions of BHB to primary intermediates that are directly used for ATP production. Metabolic pathways of BHB outside of primary metabolism have not been reported to date.

Jansen et al. previously showed that CNDP2 (carnosine dipeptidase 2) catalyzes the condensation of lactate and amino acids *in vitro*,[10] and we established this biochemical pathway to be a physiologically relevant synthetase reaction *in vivo*.[11] The most abundant member of the *N*-lactoyl amino acids, *N*-lactoyl-phenylalanine (Lac-Phe), is an exercise- and metformin-inducible metabolite that suppresses food intake and body weight.[12,13] These data show that the metabolic pathways of lactate extend beyond glycolysis and primary metabolism and include secondary metabolic shunt pathways that produce lactate-derived signaling metabolites. From a chemical perspective, BHB and lactate exhibit a high degree of structural similarity: both are hydroxy fatty acids that differ only by a single methylene. We therefore considered the possibility that BHB, like lactate, might also be enzymatically conjugated to amino acids. This predicted metabolic pathway would represent a previously unknown pathway of BHB secondary metabolism and produce a class of orphan metabolites, the *N*-β-hydroxybutyryl amino acids (BHB-amino acids). However, we were unable to find any evidence for enzymatic BHB-ylation of free amino acids in the published literature. We also were unable to find prior annotation of any BHB-amino acids as endogenous metabolites in public databases such as METLIN,[14] the Human Metabolome Database (HMDB),[15] or Global Natural Product Social Molecular Networking (GNPS).[16]

Here, we show that the enzyme CNDP2 catalyzes BHB-ylation of free amino acids *in vitro* and *in vivo*. The product of this biochemical reaction, the BHB-amino acids, are endogenously present in mouse and human plasma and exhibit ketosis inducibility and genetic regulation. *N*-β-hydroxybutyryl phenylalanine (BHB-Phe), the most abundant BHB-amino acid, is a structural and functional congener of Lac-Phe that suppresses feeding upon administration to obese mice. Conversely, CNDP2-knockout (KO) mice exhibit increased food intake and body weight on a ketogenic diet or following ketone ester administration. Lastly, CNDP2-mediated amino acid BHB-ylation and the BHB-amino acid metabolites are conserved in humans. These data establish a BHB metabolic shunt pathway linked to energy balance.

RESULTS

CNDP2 catalyzes BHB-ylation of amino acids *in vitro*

To determine whether CNDP2 can catalyze the BHB-ylation of amino acids *in vitro* (Figure 1A), we incubated BHB and phenylalanine (20 mM each) with cell lysates from HEK293T cells that were transiently transfected with FLAG-tagged mouse CNDP2 or GFP control. Overexpression of CNDP2 protein was confirmed by western blotting (Figure S1A). After incubation at 37°C for 1 h, we used liquid chromatography-mass spectrometry (LC-MS) to measure the expected condensation product, BHB-Phe. As shown in Figure 1B, CNDP2-transfected cell lysates exhibited >140-fold greater phenylalanine BHB-ylation activity compared with GFP-transfected cell lysates. CNDP2 can therefore synthesize BHB-Phe, in addition to its previously reported Lac-Phe synthesis activity. We performed several control experiments to examine the substrate specificity of the CNDP2-dependent BHB-ylation reaction. CNDP2 exhibited similar rates of amino acid BHB-ylation and *N*-lactoylation but could not accept shorter (e.g., acetate, C2) or longer (e.g., octanoate, C8) organic acids as substrates (Figure 1C). On the amino acid side, CNDP2 exhibited the fastest BHB-ylation activity using phenylalanine as a substrate (Figure 1D). Some other hydrophobic amino acids were also accepted, but with lower activity (<20%) compared with phenylalanine, and no activity was observed with many of the amino acids tested (Figure 1D). CNDP2 did not exhibit BHB-ylation of the free N terminus of a peptide substrate (Figure S1B). CNDP2 was also unable to accept the BHB isomer 3-hydroxyisobutyrate (3-HIB) acid as a substrate, though we did observe minor CNDP2 condensation activity with 2-hydroxybutyrate (2-HB) (Figure S1C).[17,18]

To quantitatively compare the kinetics of CNDP2-dependent BHB-ylation and *N*-lactoylation, we generated purified recombinant mouse CNDP2-FLAG protein for *in vitro* kinetic assays. The resulting kinetic data, which were fit to Michaelis-Menten kinetics, revealed that BHB is in fact a higher-affinity substrate for the CNDP2 active site than lactate (K_m for BHB = 8.8 mM; K_m for lactate = 33.4 mM, Figures 1E and 1F). By contrast, CNDP2-dependent Lac-Phe synthesis is faster than that of BHB-Phe synthesis under conditions of saturating substrate concentrations (V_{max} for lactate = 62.7 nM/min/mg, V_{max} for BHB = 3.5 nM/min/mg, Figures 1E and 1F).

Lastly, we docked the product BHB-Phe into the CNDP2 active site (Figure 1G; see STAR Methods). This modeling predicted several interactions of BHB-Phe with key active site residues, including E166, D195, and H455. We generated single-point mutations of each of these residues by transient transfection to HEK293T cells (Figure S1D). In each case, mutations of any of these active site residues concomitantly reduced both CNDP2-dependent BHB-Phe and Lac-Phe production (Figures 1H and 1I). Therefore, BHB-ylation and *N*-lactoylation activities are both entirely encoded within the CNDP2 polypeptide. In addition, these two catalytic activities cannot be readily dissociated by single-point mutations in the active site pocket.

CNDP2-dependent BHB-ylation in mouse tissues

To determine whether endogenous CNDP2 catalyzes amino acid BHB-ylation in mouse tissues, we first examined the tissue expression of CNDP2 by western blot using an anti-CNDP2 antibody. The specificity of this antibody was confirmed using tissues from CNDP2-KO mice (Figure S2A). CNDP2 protein levels were highest in kidney and gut and lower in many of the other tissues examined (Figure 2A). Next, we performed *in vitro* BHB-Phe

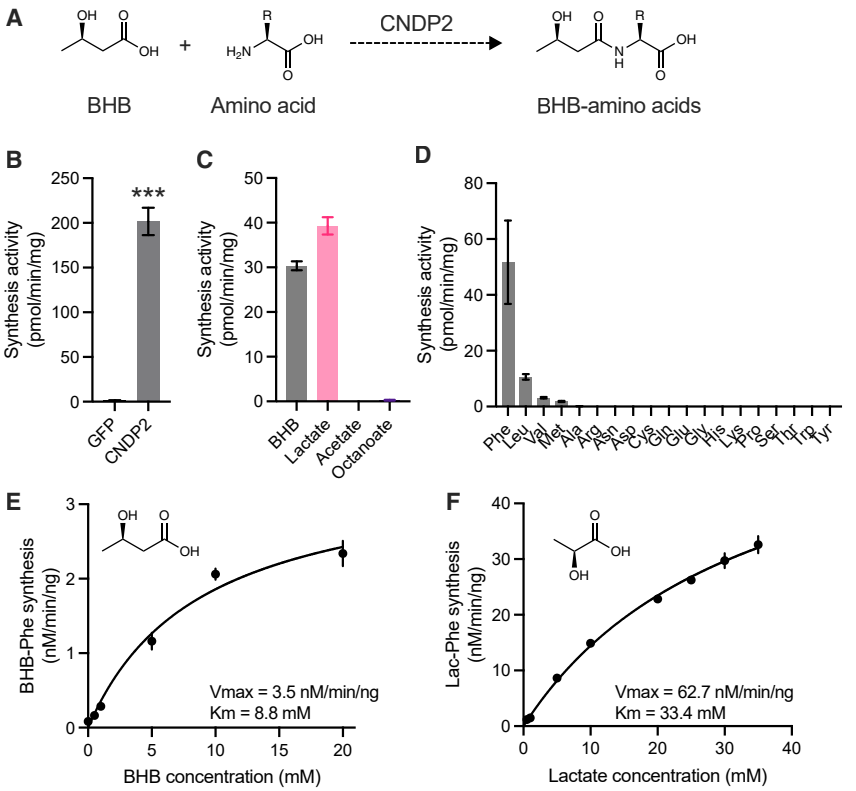

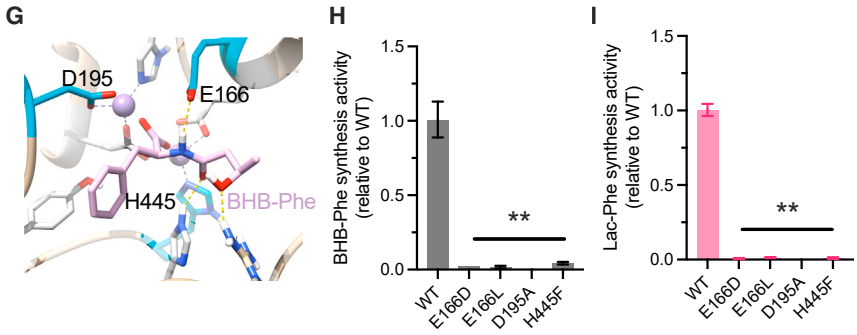

Figure 1. CNDP2 catalyzes amino acid BHB-ylation *in vitro*

(A) Schematic of CNDP2-dependent Lac-Phe synthesis and the proposed CNDP2-dependent BHB-Phe synthesis reaction.

(B) BHB-Phe synthesis activity of cell lysates transfected with GFP or mouse CNDP2-FLAG.

(C and D) Synthesis activity of cell lysates transfected with GFP or mouse CNDP2-FLAG and incubated with the indicated monocarboxylate with Phe (C) or the indicated amino acid with BHB (D).

(E and F) Michaelis-Menten kinetics of recombinant purified mouse CNDP2-FLAG protein with BHB (E) or lactate (F) as the organic acid donor.

(G) Molecular docking of BHB-Phe into the mouse CNDP2 active site.

(H and I) BHB-Phe synthesis activity (H) or Lac-Phe synthesis activity (I) of HEK293T cells transfected with the indicated mouse WT or mutant CNDP2 plasmid.

For enzyme assays, organic acids and amino acids were incubated at a concentration of 20 mM at 37°C for 1 h. For (B)–(F), (H), and (I), $n = 3$–4/group. Data for (B)–(F), (H), and (I) are shown as means ± SEM. p values were calculated by Student's two-sided t test.

See also Figure S1.

synthesis activity using crude total lysates of kidney, gut, brain, liver, and quadriceps tissues from wild-type (WT) mice (see STAR Methods). We selected these tissues because of their wide range of CNDP2 protein expression. As shown in Figure 2B, the highest BHB-Phe synthesis activity was observed in kidney and gut (~10–30 pmol/min/mg), whereas brain, liver, and quadriceps exhibited lower, but detectable, BHB-Phe synthesis activity (~1–5 pmol/min/mg). This pattern of BHB-Phe synthesis across tissues largely paralleled the protein expression of CNDP2 in these same tissues. In addition, the temperature dependence of the renal BHB-Phe synthesis activity also paralleled that of recombinant CNDP2 protein (Figures S2B and S2C). Therefore, the tissue expression pattern and temperature profile of CNDP2 protein both correlate with the tissue BHB-Phe synthesis activity.

We used tissues from CNDP2-KO mice to determine the contribution of CNDP2 to the tissue BHB-Phe synthesis activity. As shown in Figure 2B, both kidney and gut BHB-Phe synthesis activity was largely abolished (>95% reduced) in tissues from CNDP2-KO mice. The smaller BHB-Phe synthesis activity in other tissues was also greatly diminished (>85% reduced in brain, >75% reduced in liver, and >60% reduced in quadriceps). Using leucine or valine as substrates for *in vitro* BHB-ylation, a similar pattern of BHB-Leu and BHB-Val synthesis across WT and CNDP2-KO tissues was observed (Figures 2C and 2D): kidney and gut tissues from WT mice both exhibited the highest BHB-amino acid synthesis activity, and this activity was largely abolished in tissues from CNDP2-KO mice. In additional control experiments, we assayed tissue Lac-Phe synthesis activity, which again exhibited a similar pattern and CNDP2 dependence to that of BHB-amino acid synthesis (Figure 2E). By contrast, carnosine hydrolysis across tissues exhibited a distinct pattern, with highest activity in liver and quadriceps and little activity in the kidney, gut, and brain (Figure 2F). Importantly, the carnosinase activity was not altered in CNDP2-KO tissues (Figure 2F). We conclude that CNDP2 is the principal enzyme responsible for BHB-amino-acid-synthesis activity in mouse tissues. In addition, despite its previously annotated *in vitro* activity, CNDP2 is not a major tissue carnosinase.

BHB-amino acids are endogenous mouse metabolites

The product of the CNDP2-catalyzed BHB-ylation reaction, BHB-amino acids, have not been previously reported as

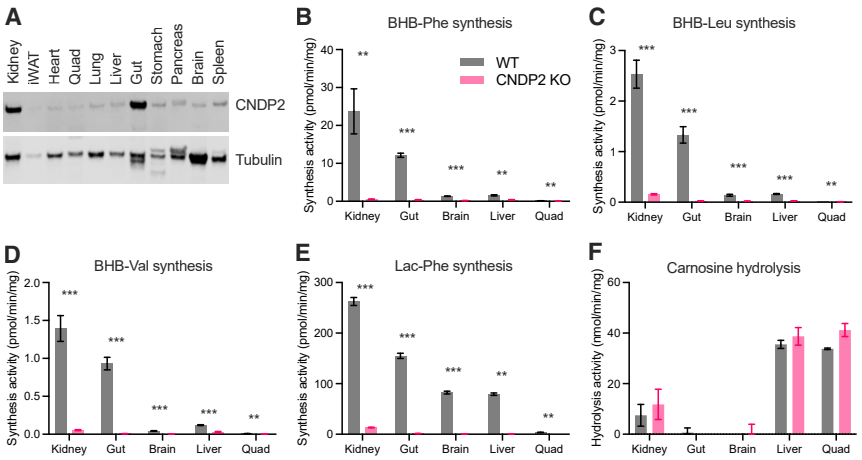

Figure 2. CNDP2 is the principal BHB-amino acid synthetase in mouse tissues

(A) Western blot of the indicated mouse tissues using an anti-CNDP2 (top) or anti-tubulin (bottom) antibody.

(B–F) Enzyme activities of tissues from WT or CNDP2-KO mice when provided with BHB and Phe (B), BHB and Leu (C), BHB and Val (D), lactate and Phe (E), or carnosine (F) as substrates.

For enzyme assays, organic acids and amino acids were incubated at a concentration of 20 mM at 37°C for 1 h.

For (B)–(F), n = 3–4/group. Data for (B)–(F) are shown as means ± SEM. p values were calculated by Student's two-sided t test.

See also Figure S2.

endogenous metabolites. We therefore developed a targeted metabolomics approach to determine whether BHB-amino acids can be detected in mouse plasma. We first synthesized an authentic BHB-Phe standard by classical amide coupling between BHB and phenylalanine (Figure 3A; see STAR Methods). Fragmentation of the authentic BHB-Phe standard revealed a major daughter ion corresponding to Phe (m/z = 164) and a second, smaller daughter ion corresponding to the decarboxylation product (m/z = 206). Next, we developed a targeted multiple reaction monitoring (MRM) method on a high-performance liquid chromatography coupled to triple quadrupole mass spectrometry (QQQ-LC/MS) to monitor the parent to phenylalanine transition for BHB-Phe. In mouse plasma, we identified an endogenous peak that eluted at an identical retention time with the authentic standard (Figure 3A). To exclude the possibility that this method may also be detecting isobaric 2-HB- and 3-HIB-phenylalanine isomers, we synthesized authentic standards of 2-HB-Phe and 3-HB-Phe and developed MRM methods that could distinguish between each of the three molecules. Although 2-HB-Phe and 3-HIB-Phe also yielded daughter ions corresponding to phenylalanine, we also identified unique transitions for each of these isomers (2-HB-Phe: 260 > 102, fragmentation at N-Cα; 3-HIB-Phe: 250 > 220, loss of CH_3O, Figures S3A and S3B). For BHB-Phe, >99% of the total signal was detected using the 250 > 164 transition, 2-HB-Phe was detected using both 260 > 102 and 250 > 164 (in a 6:1 ratio), and 3-HIB-Phe was detected using both 250 > 220 and 250 > 164 (in a 1.6:1 ratio) (Figure S3C). The signal from the endogenous peak was found to be comprised >99% of the 260 > 164 transition (Figure S3C). Therefore, the endogenous signal is BHB-Phe; in addition, 2-HB-Phe and 3-HIB-Phe are not endogenous metabolites.

We next synthesized authentic standards for BHB-Leu, BHB-Val, and BHB-Met, which also exhibited the same characteristic amino acid daughter ion (Figures 3B–3D). Using a similar MRM approach, we also detected endogenous peaks with transition and retention time identical to that of the authentic standards (Figures 3B–3D), demonstrating that these other BHB-amino acids are also endogenous metabolites.

Because of their biosynthetic origin from BHB, circulating BHB-amino acids would be predicted to rise with increasing BHB levels, such as those achieved by nutritional or physiologic ketosis. Levels of BHB-amino acids in mouse blood plasma were therefore measured after 1 week of ketogenic diet, a 24-h fast, or oral administration of a ketone ester drink (3 g/kg of body weight). We confirmed that plasma BHB levels were elevated by each of these conditions (Figure S3D). All these stimuli consistently produced robust 2- to 10-fold elevations in each of the BHB-amino acids (Figures 3E–3H). Ketogenic diet produced greater variation in induction of BHB-amino acid levels, which may reflect the more chronic nature of this perturbation (1 week) compared with the two other acute ketosis stimuli (≤ 24 h). The levels of phenylalanine, Lac-Phe, and lactate were not consistently changed across the three ketosis stimuli (Figure S3D). Tissue levels of BHB-Phe were also detectable and elevated after ketone ester oral gavage (Figure S3E). We conclude that BHB-amino acids are endogenous, ketosis-inducible mouse metabolites.

Genetic regulation of BHB-amino acids by CNDP2 and HMGCL

Figure 4A shows a schematic of the CNDP2-dependent ketone metabolic shunt pathway in the context of known ketogenesis and ketolysis pathways. To directly test the physiologic contribution of CNDP2 to BHB-amino acid biosynthesis, we measured BHB-amino acids in blood plasma from CNDP2-KO mice after a ketone ester drink challenge or after 1 week of ketogenic diet. After acute administration of ketone ester drink, CNDP2-KO mice exhibited >90% depletion of multiple plasma BHB-amino acids (Figure 4B). Reductions in multiple BHB-amino acids were also observed in CNDP2-KO mice after 1 week on a ketogenic diet (Figure 4C). In both experiments, levels of plasma BHB, lactate, or phenylalanine were not consistently changed between WT and CNDP2-KO mice, and levels of Lac-Phe were, as expected, reduced in CNDP2-KO mice (Figures S4A and S4B).

We performed additional metabolomic profiling of organic acid-amino acid conjugates in CNDP2-KO mice. N-acetyl-Phe, N-acetyl-Val, N-acetyl-Leu, and N-acetyl-Met, as well as their corresponding free amino acids, were not changed between WT and CNDP2-KO mice (Figure S4C). We were unable to detect N-propyl, N-butyryl, or N-octanoyl-amino acids (C3, C4, and C8,

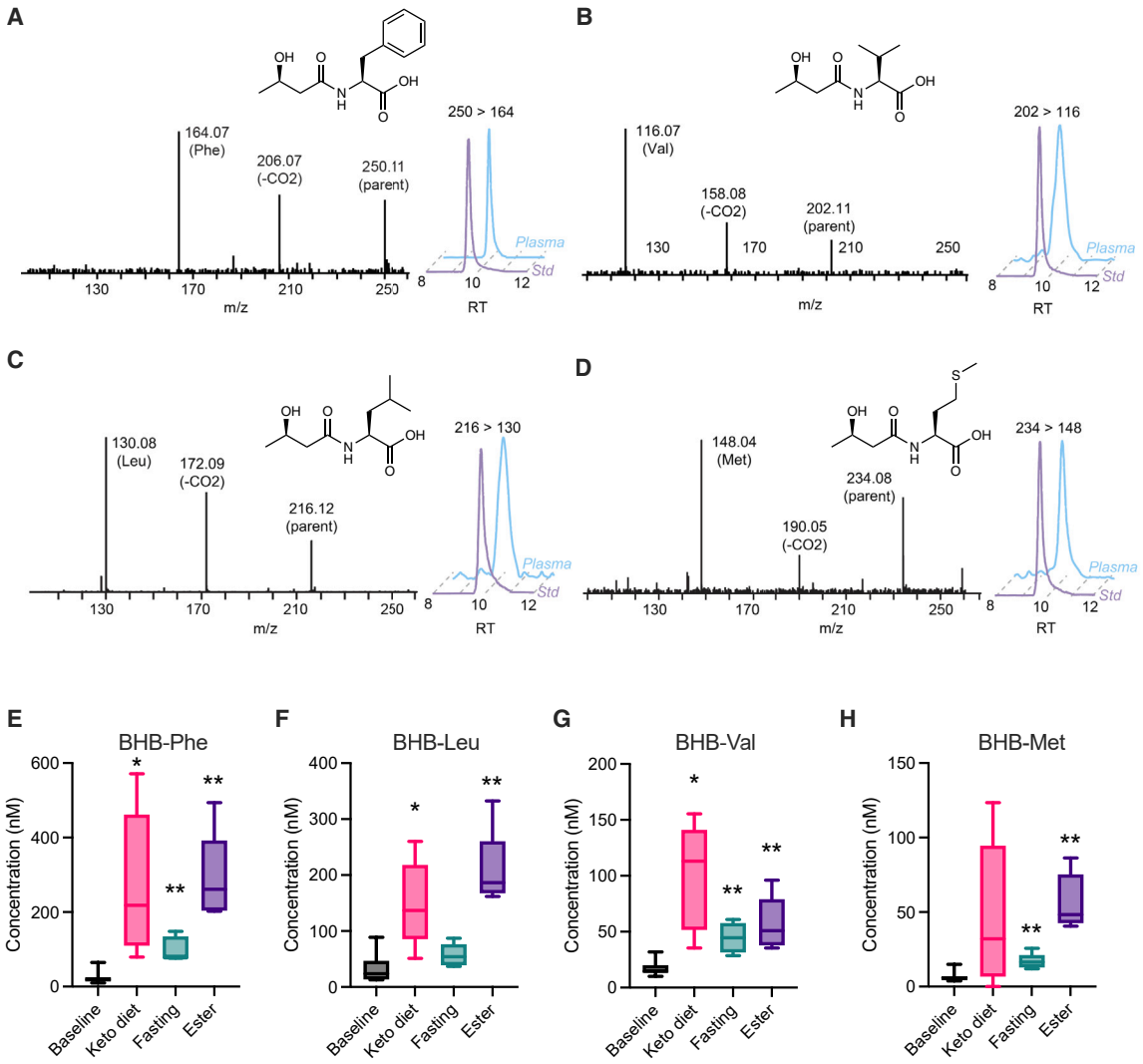

Figure 3. Detection and ketosis inducibility of BHB-amino acids in mouse plasma

(A–D) Tandem mass spectrometry fragmentation of the authentic standard (left) and co-elution of the standard and the endogenous peak from mouse plasma (right) using the indicated multiple reaction monitoring transition for BHB-Phe (A), BHB-Val (B), BHB-Leu (C), and BHB-Met (D).

(E–H) BHB-amino acid quantitation in 8- to 9-week-old male C57BL/6J mouse plasma at baseline, after 1 week on a ketogenic diet (Research Diets D21021803), after a 24-h fast, or 30 min post ketone monoester drink administration by oral gavage (3 g KE/kg of body weight).

For (E)–(H), n = 5/group, with the baseline n = 15 (pooled from each of the three groups). Data for (E)–(H) are shown as box-and-whisker plots. p values were calculated by Student's two-sided t test.

See also Figure S3.

respectively, Figure S4C), likely reflecting the low circulating abundance of the corresponding organic acids compared with acetate, lactate, and BHB.

Next, we examined the effects of liver-specific deletion of HMGCL, a critical upstream enzyme in hepatic ketogenesis (Figure 4A). We obtained plasma from liver-specific KOs of HMGCL (*Alb-Hmgcl*$^{-/-}$ mice), which were previously generated by crossing *Albumin*-cre mice with *Hmgcl*$^{fl/fl}$ mice.[7] Several BHB-amino acids, such as BHB-Met, BHB-Leu, and BHB-Val, but not BHB-Phe, were reduced by ~50%–80% in plasma from these animals (Figure 4D). We confirmed ~30% reductions in BHB levels in plasma from *Alb-Hmgcl*$^{-/-}$ mice and, in addition, found no changes in lactate, Lac-Phe, or phenylalanine levels compared with *Hmgcl*$^{fl/fl}$ controls (Figure S4D). Together, these data establish the genetic and biochemical requirement for two upstream enzymes, HMGCL and CNDP2, in the regulation of circulating BHB-amino acids levels.

Role of BHB-Phe in feeding behaviors and body weight regulation

BHB-Phe is the most abundant BHB-amino acid (Figure 3E). This metabolite is a congener of Lac-Phe that shares both chemical

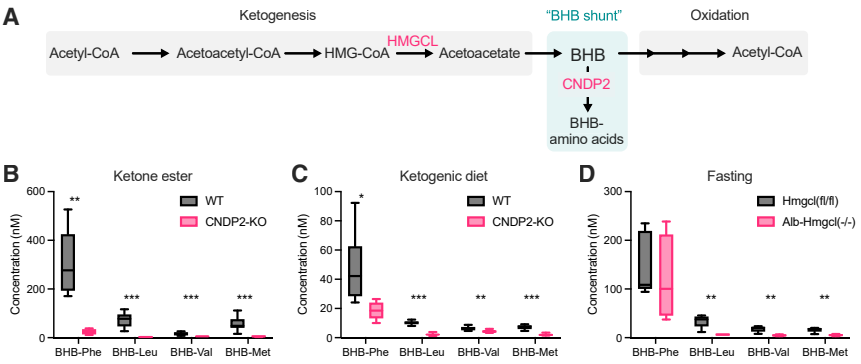

Figure 4. Genetic regulation of BHB-amino acids by CNDP2 and HMGCL

(A) Schematic of ketone biochemical pathways and the genetic mouse models used.

(B–D) BHB-amino acid quantitation in plasma from 4- to 10-week-old male WT and CNDP2-KO mice at 60 min post ketone monoester drink administration by oral gavage (3 g KE/kg of body weight) (B), from 7- to 16-week-old female WT and CNDP2-KO mice after 1 week on a ketogenic diet (Research Diets D06040601, C), or from *Hmgcl*$^{fl/fl}$ vs. *Alb-Hmgcl*$^{-/-}$ mice after a 24-h fast (D). For (B), $n = 7$ for WT and 4 for KO. For (C), $n = 8$ per group. For (D), $n = 5$ for *Hmgcl*$^{fl/fl}$, $n = 4$ for *Alb-Hmgcl*$^{-/-}$. Data for (B)–(D) are shown as box-and-whisker plots. p values were calculated by Student's two-sided t test.

See also Figure S4.

similarity as well as a common biosynthetic pathway via CNDP2. We therefore considered the possibility that BHB-Phe might also be functionally similar to Lac-Phe and regulate food intake and body weight. We first used gain-of-function approaches to determine whether BHB-Phe is sufficient to reduce food intake and body weight. In an initial study of diet-induced obese (DIO) mice in metabolic chambers, BHB-Phe (50 mg/kg, intraperitoneally [i.p.]) reduced food intake without affecting movement, oxygen consumption, or carbon dioxide production (Figures 5A–5E). A reduction in respiratory exchange ratio (RER) was also observed, consistent with a suppression of food intake (Figure 5E). Under these conditions, plasma BHB-Phe levels peaked at ~20 μM at the 1-h time point and returned to baseline values by 3 h (Figure S5A). In an independent experiment in home cages, we found that acute administration of BHB-Phe (50 mg/kg, i.p.) to DIO mice suppressed food intake without affecting water intake, establishing specific suppression of food vs. fluid ingestion (Figure S5B). Lastly, plasma levels of other feeding-regulating hormones, such as ghrelin, leptin, and GDF15, were also unaltered in mice following a single administration with BHB-Phe (50 mg/kg, i.p., Figure S5C).

We performed chronic studies of BHB-Phe in DIO mice. Daily administration of BHB-Phe (50 mg/kg/day, i.p.) resulted in a durable suppression of daily food intake and, as expected, a concomitant reduction in body weight gain (Figures 5F and 5G). At the end of the experiment, BHB-Phe-treated mice exhibited reductions in aspartate aminotransferase (AST), alanine aminotransferase (ALT), and total triglycerides (TGs); no changes were found in high-density lipoprotein (HDL)- or low-density lipoprotein (LDL)-cholesterol (Figure S5D). BHB-Phe-treated mice lost the same amount of weight as pair-fed controls (Figure 5H), demonstrating that the observed suppression of food intake explains the observed change in body weight in BHB-Phe-treated mice.

To understand the structural requirements of BHB-Phe that are important for its body weight-lowering effects, we tested the effect of additional, structurally related metabolites. First, although BHB-Phe (50 mg/kg/day, i.p.) efficiency suppressed body weight and food intake in DIO mice, either BHB alone or phenylalanine alone at the same doses were without effect (Figure 5I). Second, the related metabolites BHB-Lys (50 mg/kg, i.p.), as well as the dipeptides Phe-Phe (50 mg/kg, i.p.) and Leu-Leu (50 mg/kg, i.p.), also failed to reduce food intake or body weight (Figures 5J and 5K). Third, we tested other CNDP2-regulated BHB conjugates, including BHB-Met, BHB-Leu, and BHB-Val. These metabolites consist of BHB conjugated to hydrophobic amino acids; notably, two of them, BHB-Leu and BHB-Val, represent BHB conjugated to branched-chain amino acids (BHB-BCAAs). In this case, we observed body-weight-lowering activity for each BHB-Met, BHB-Leu, and BHB-Val (Figure S5E). Therefore, BHB-Phe and other CNDP2-regulated BHB-hydrophobic amino acid conjugates, including BHB-BCAAs, have anorexigenic and anti-obesity effects in mice, whereas BHB conjugates to other essential amino acids such as BHB-Lys, as well as other dipeptides, do not exhibit the same bioactivity.

Lastly, we used CNDP2-KO mice to examine the physiologic contributions of BHB-amino acids to energy balance. We previously reported a gene-by-environment interaction of the *Cndp2* gene and glycolytic stimuli: CNDP2-KO mice have normal body weights after a standard high-fat-diet feeding protocol; however, upon glycolytic stimulus challenge to increase Lac-Phe levels (by treadmill exercise or by metformin treatment), KO animals exhibit an increased food intake and body weight phenotype compared with WT controls.[11,12] To determine the contribution of BHB-amino acids, in an initial experiment we administered ketone esters (3 g/kg/day, per os [p.o.]) to WT and CNDP2-KO mice that had been rendered obese by high-fat-diet feeding for 11–19 weeks. At the beginning of the experiment, body weights were not different between genotypes. By the end of the 12-day ketone ester treatment, WT mice on average lost −0.3 ± 0.4 g, whereas CNDP2-KO mice gained +1.0 ± 0.2 g (mean ± SEM, $p < 0.05$, Figure 5L). CNDP2-KO mice also exhibited greater cumulative food intake than WT mice (Figure 5M). In a second experiment, we placed WT and CNDP2-KO mice on a ketogenic diet. Initial body weights were once again not different between genotypes. By the end of the experiment, CNDP2-KO mice on a ketogenic diet gained more weight and ate more food than WT mice (Figure S5F). We confirmed that Lac-Phe and BHB-Phe were independently induced following sprint treadmill exercise and ketone ester or ketogenic diet treatment, respectively (Figure S5G). Therefore, ketone esters

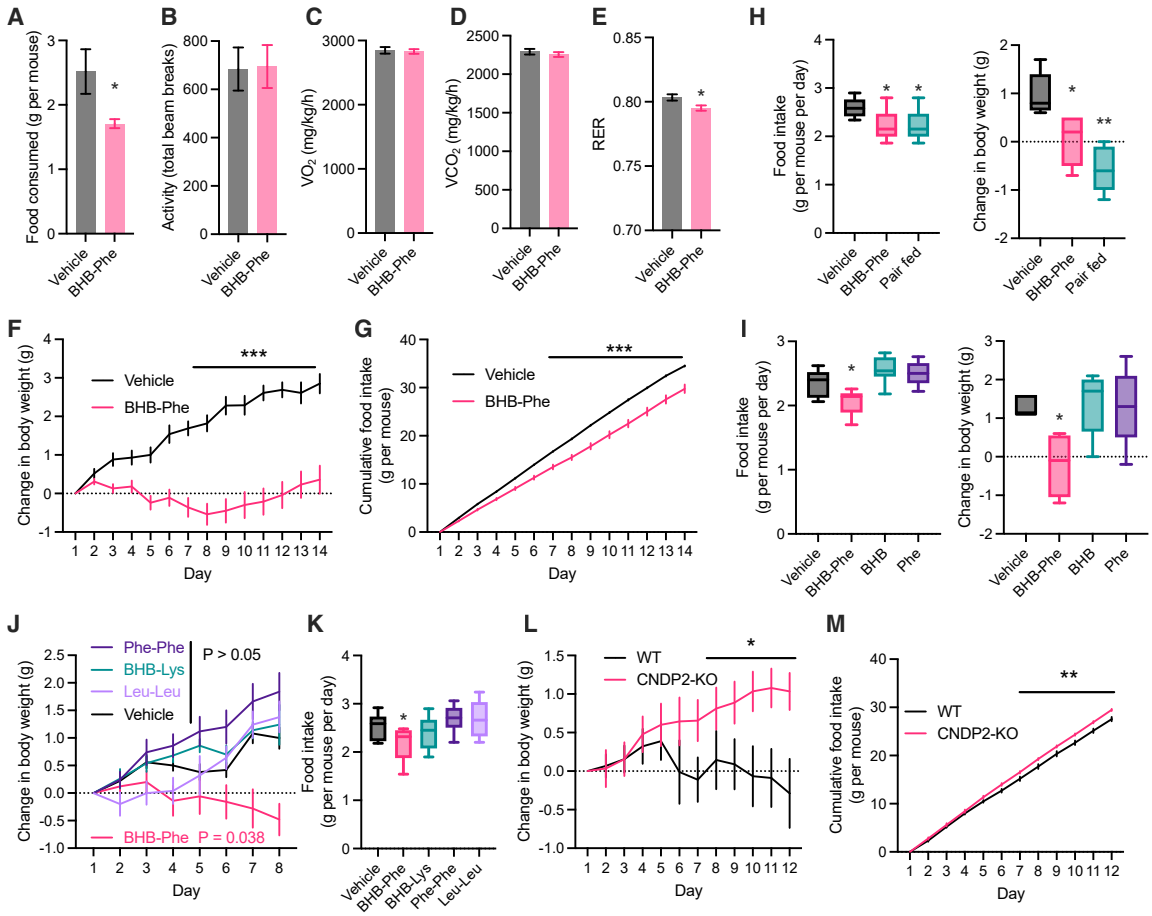

Figure 5. BHB-Phe suppresses food intake and body weight

(A–E) Food intake (A), ambulatory movement (B), oxygen consumption (VO_2) (C), carbon dioxide production (VCO_2) (D), and respiratory exchange ratio (RER) (E) of singly housed 29-week-old male DIO mice following a single injection of vehicle or BHB-Phe (50 mg/kg, i.p.) over a 10-h period in metabolic chambers.

(F and G) Change in body weight (F) and cumulative food intake (G) of singly housed 28-week-old male DIO mice treated with vehicle or BHB-Phe (50 mg/kg/day, i.p.). Starting body weights were vehicle: 46.4 ± 1.4 g, BHB-Phe 45.7 ± 1.0 g (mean ± SEM).

(H) Change in body weight (left) and daily food intake (right) of group-housed 15-week-old male DIO mice after 6 days of treatment with vehicle, BHB-Phe (50 mg/kg/day, i.p.), or vehicle-treated pair-fed mice. Starting body weights were vehicle: 39.4 ± 2.3 g, BHB-Phe: 38.5 ± 0.8 g, and pair-fed: 37.8 ± 0.6 g (mean ± SEM).

(I) Change in body weight (left) and food intake (right) of group-housed 13-week-old male DIO mice after 9 days of treatment with vehicle, BHB-Phe, BHB, or phenylalanine (50 mg/kg/day, i.p.). Starting body weights were vehicle: 36.2 ± 0.7 g, BHB-Phe: 37.9 ± 2.1 g, BHB: 36.8 ± 1.1 g, Phe: 34.5 ± 0.5 g (mean ± SEM).

(J and K) Change in body weight (J) and food intake (K) of group-housed 14- to 16-week-old male DIO mice after 9 days of treatment with Phe-Phe, BHB-Lys, Leu-Leu, BHB-Phe (50 mg/kg/day i.p.), or vehicle. Starting body weights were vehicle: 41.2 ± 1.3 g, BHB-Phe: 39.1 ± 1.7 g, BHB-Lys: 40.1 ± 2.2 g, Phe-Phe: 40.8 ± 1.4 g, Leu-Leu: 41.2 ± 1.3 g (mean ± SEM).

(L and M) Change in body weight (L) and food intake (M) of singly housed 19- to 32-week-old male WT and CNDP2-KO mice that had been rendered obese by high-fat-diet feeding for 11–19 weeks receiving ketone esters (3 g/kg/day, per os [p.o.]). Starting body weights were WT: 46.8 ± 1.4 g, CNDP2-KO: 47.1 ± 1.3, $p > 0.05$ (mean ± SEM).

For (A)–(E), $n = 7$ for vehicle, $n = 8$ for BHB-Phe. For (F) and (G), $n = 10$ per group. For (H)–(K), $n = 5$ per group. For (L) and (M), $n = 9$ per group. Data in (A)–(G), (J), (L), and (M) are shown as the mean ± SEM. Data in (H), (I), and (K) are shown as box-and-whisker plots. p values were calculated by Student's two-sided t test or by two-way ANOVA.

See also Figure S5.

and a ketogenic diet represent environmental perturbations that uncover the effects of *Cndp2* genotype on body weight and food intake.

BHB-Phe activates neural populations in the hypothalamus and brainstem

To better understand the neurobiological mechanisms by which BHB-Phe suppresses feeding, we first used pharmacological and genetic approaches to determine whether the effect of BHB-Phe might be mediated by hypothalamic melanocortin signaling, glucagon-like peptide-1 receptor (GLP-1R), or brainstem GDNF family receptor alpha-like (GFRAL) pathways. The effect of BHB-Phe (50 mg/kg, i.p.) on food intake and body weight was similar in WT or melanocortin 4 receptor (MC4R)-KO mice (Figures S6A and S6B). Similarly, the GLP-1R antagonist Exendin-3 (0.1 mg/kg/day, i.p.) efficiently blocked the

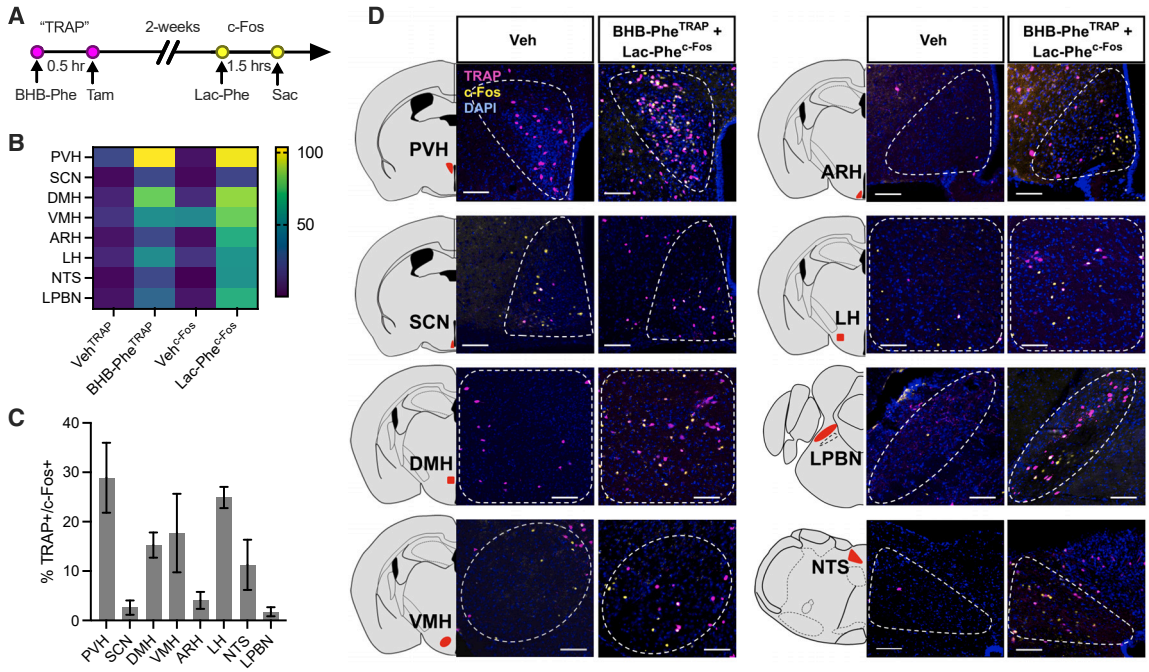

Figure 6. TRAP/c-Fos mapping of BHB-Phe- and Lac-Phe-activated neurons in the brain

(A) A schematic diagram of the experimental design for mapping BHB-Phe- and Lac-Phe-activated neurons. TRAP, targeted recombination in active populations.

(B) Heatmap showing the number of Veh^{TRAP}-, BHB-Phe^{TRAP}-, Veh$^{c\text{-}Fos}$-, and Lac-Phe$^{c\text{-}Fos}$-labeled neurons in various brain regions. ARH, arcuate nucleus of the hypothalamus; DMH, dorsomedial hypothalamus; LH, lateral hypothalamus; LPBN, lateral parabrachial nucleus; NTS, nucleus of the solitary tract; PVH, paraventricular hypothalamus; SCN, suprachiasmatic nucleus; VMH, ventromedial hypothalamus.

(C and D) Quantification (C) and representative sections (D) of TRAP+/c-Fos+ neurons in the indicated brain regions.

For (B) and (C), n = 3 per group. Data in (C) are shown as mean ± SEM. Scale bars, 100 μm.

See also Figures S6 and S7.

anorexigenic and anti-obesity effects of GLP-1 (2 mg/kg/day, i.p., Figures S6C and S6D); however, under these same Exendin-3 did not alter the effect of BHB-Phe on food intake and body weight (Figures S6E and S6F). We obtained a neutralizing anti-GFRAL antibody[19,20] (Eli Lilly clone 8A2) and verified that this antibody (10 mg/kg, subcutaneously [SQ]) completely blocked the activity of recombinant GDF15 to suppress food intake and body weight (4 nmol/kg, SQ) (Figure S6G); however, the effect of BHB-Phe on feeding and body weight was unaffected by anti-GFRAL antibody administration (Figures S6H and S6I). We conclude that the anorexigenic activity of BHB-Phe is independent of these known pathways of feeding control.

Next, we used an activity-dependent genetic labeling strategy[21] (TRAP, targeted recombination in active populations) to identify neurons activated following pharmacological dosing of BHB-Phe. In this approach, upon BHB-Phe treatment, c-Fos-dependent recombination of a reporter cassette (tdTomato) enables permanent genetic labeling of BHB-Phe. We treated TRAP2 mice (TRAP2/Rosa26-LSL-tdTomato) with BHB-Phe (50 mg/kg, i.p.), followed by 4-hydroxytamoxifen 30 min later, to initiate cre-dependent recombination in BHB-Phe-activated neurons. 2 weeks later, the same mice received Lac-Phe (50 mg/kg, i.p.) and were sacrificed 90 min later for c-Fos immunostaining (Figure 6A). This experimental approach therefore enables concurrent identification of both BHB-Phe-activated (e.g., TRAP+, marked by tdTomato) and Lac-Phe-activated (e.g., c-Fos+) neurons in the same animal. We examined multiple hypothalamic and brainstem regions for TRAP+ or c-Fos+ neurons. Compared with vehicle treatment, BHB-Phe and Lac-Phe both activated neuronal populations in multiple brain regions, including the paraventricular hypothalamic nucleus (PVH), the suprachiasmatic nucleus (SCN), the dorsomedial hypothalamic nucleus (DMH), the ventromedial hypothalamic nucleus (VMH), the arcuate nucleus of the hypothalamus (ARH), the lateral hypothalamus (LH), the lateral parabrachial nucleus (LPBN), and the nucleus of the solitary tract (NTS) (Figure 6B). Detailed analyses of TRAP+ neurons and c-Fos+ neurons in each of these regions revealed that only a small fraction (~2%–30%) of neurons were activated by both BHB-Phe and Lac-Phe (e.g., double TRAP+/c-Fos+), whereas the vast majority of activated neurons were distinct (Figure 6C). Representative sections from the indicated regions are shown in Figure 6D. Because TRAP recombination and c-Fos immunoreactivity may have different sensitivities to label-activated neurons, we repeated this experiment in an independent cohort of TRAP2/Rosa26-LSL-tdTomato mice but now reversed the BHB-Phe/Lac-Phe sequence. In this reversed experiment, Lac-Phe-activated neurons were identified by TRAP recombination, whereas BHB-Phe-activated neurons were identified by c-Fos immunoreactivity (Figure S7A). Once again, although both Lac-Phe and BHB-Phe activated neural

populations in the hypothalamus and brainstem (Figure S7B), detailed analysis of each region showed that the two populations of activated neurons were largely distinct (Figure S7C). We conclude that pharmacological administration of BHB-Phe activates several hypothalamic and brainstem regions implicated in feeding behaviors in a manner overlapping but distinct from that of Lac-Phe.

Conservation of CNDP2 enzyme activity and BHB-amino acids in humans

Lastly, we sought to understand the conservation of the CNDP2-dependent amino acid BHB-ylation pathway to humans. First, we obtained recombinant human CNDP2, which exhibited the expected *in vitro* BHB-ylation activity, using BHB and phenylalanine as substrates (Figure 7A). Michaelis-Menten kinetics using increasing concentrations of BHB also revealed similar substrate affinity and maximal velocity to the mouse CNDP2 enzyme (Figure 7B). Next, we identified three human cell lines expressing hCNDP2: U937 macrophage cells, Caco-2 gut epithelial cells, and PANC-1 pancreatic ductal cells. For each human cell line, we generated control and hCNDP2-KO lines via CRISPR-Cas9. Complete loss of hCNDP2 was validated by western blotting using our anti-CNDP2 antibody (Figures 7C–7E). Knockout of hCNDP2 in each cell line resulted in near complete ablation of cell lysate BHB-amino-acid-synthesis activity. These data show that an endogenous amino acid BHB-ylation activity is present in human cells and primarily mediated by CNDP2 (Figures 7C–7E). Lastly, to determine whether BHB-amino acids are endogenous human metabolites, we measured plasma levels of BHB-amino acids from a subset of participants in a trial of exogenous ketone supplementation.[22] After fasting overnight (>8 h), participants consumed a ketone monoester drink (0.3 g/kg HVMN Ketone Ester) and plasma was collected 1 h later. BHB-Phe, BHB-Leu, BHB-Val, and BHB-Met were also detectable in baseline plasma samples and elevated after ketone ester drink (Figure 7F). As expected, levels of BHB were increased by the ketone ester drink, whereas levels of phenylalanine, Lac-Phe, and lactate remained unchanged (Figure 7G). Therefore, both CNDP2-mediated amino acid BHB-ylation and BHB-amino acid metabolites are conserved in humans.

DISCUSSION

Here, we show that CNDP2 controls a secondary pathway of BHB metabolism leading to the production of a family of BHB-derived metabolites, the BHB-amino acids. In addition, BHB-Phe, the most abundant BHB-amino acid, is a structural and functional congener of Lac-Phe that reduces food intake and body weight. These data establish that the biochemical pathways of BHB extend beyond primary metabolic intermediates and include BHB-derived signaling metabolites that regulate energy homeostasis.

That CNDP2 can accept either BHB or lactate as a substrate represents an unusual biochemical mechanism that directly couples a metabolic state with the production of bioactive metabolites. To the best of our knowledge, such a multi-functional, flux-dependent enzyme-coupling mechanism has not been previously described. One interpretation of these data is that CNDP2 functions a "sensor" of glycolytic or ketosis flux, depending on whether lactate or BHB levels are elevated. Interestingly, the effector is simply a metabolic derivative of the substrate and, therefore, represents one of the simplest models by which a signal can be converted to an effector.

The chemical logic of CNDP2-dependent BHB-amino acid biosynthesis mirrors that of other signaling molecule: in every case, lower-abundance bioactive species are produced from higher-abundance precursors. For instance, steroid hormones are produced from cholesterol, thyroid hormones are produced from tyrosine, prostaglandins are produced from fatty acids, and histamine is produced from histidine. Our data show that the pool of abundant precursors is not limited to amino acids, cholesterol, or lipids but can also include other abundant metabolic fuels such as BHB. In addition, this CNDP2-dependent mechanism is operational in *Cndp2*+ cells (e.g., macrophages, other immune cells, and epithelial cells of kidney and gut), which are cell types not classically associated with BHB metabolism.

Although past studies have reported the anorexigenic and anti-obesity effects associated with elevated ketones in mice[23,24] and in humans,[25] this is by no means a consolidated phenomenon. Our data demonstrate that the effects of BHB also extend to BHB-derived metabolites. Therefore, potential variations in levels of BHB-amino acids may be an important contributor to the conflicting associations of ketosis and energy balance reported in previous studies. Indeed, our own data demonstrate that changes in the circulating BHB-amino acid levels are correlated to, but not linearly determined by, changes in circulating levels of BHB itself; consequently, control for variation in BHB-amino acid levels (and potentially *CNDP2* genotype) should be potentially considered in future studies of ketosis and obesity. From a teleological point of view, high ketone levels are a product of both increased hepatic ketogenesis and adipose lipolysis to provide fatty acid substrates. Consequently, a high ketone state demonstrates that sufficient adipose lipid stores are available for ketogenesis. Therefore, one potential interpretation of the association of high ketones and food intake suppression may be that ketones, and BHB-amino acids, signal a state of fat sufficiency. In addition, our data point to hypothalamic and brainstem neural populations as potential downstream targets of BHB-Phe.

Our studies here also expand our understanding of the gene-by-environment interactions in energy balance. Previously, we had shown that CNDP2-KO mice only exhibit a body weight phenotype following treadmill running or metformin treatment but not under "standard" high-fat-diet feeding conditions. Therefore, phenotypes associated with the *Cndp2* gene are only revealed when the appropriate and specific environmental stimulus is provided. Our studies identify ketone ester administration and a ketogenic diet as environmental contributors to the CNDP2-dependent phenotype and suggest that additional nutritional or physiologic perturbations that increase ketogenesis may be relevant environmental stimuli that interact with the *Cndp2* gene.

There are two reasons why BHB-amino acids were robustly detectable in our mass spectrometry analysis but not annotated in prior metabolomic studies. First, our enzymological studies of CNDP2, and the close chemical parallels between lactate and

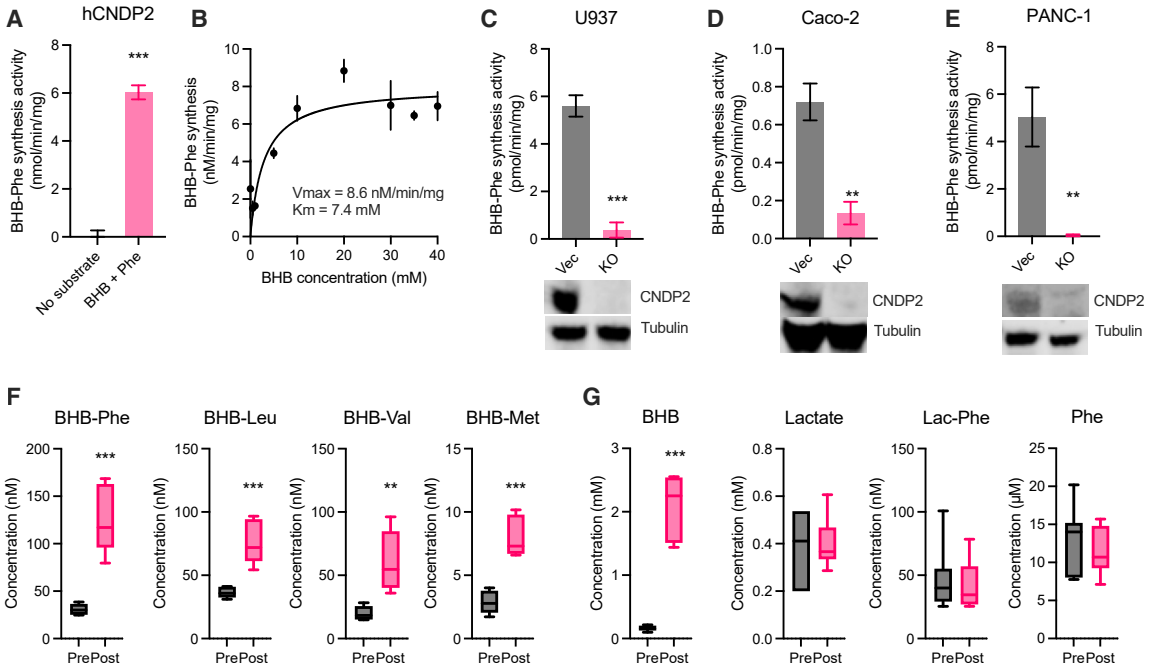

Figure 7. Human CNDP2 activity and BHB-amino acids in human plasma

(A and B) BHB-Phe synthetase activity of recombinant human CNDP2 provided with the indicated substrates (A) and Michaelis-Menten kinetics of recombinant human CNDP2 protein with increasing concentrations of BHB substrate (B).

(C–E) Top: BHB-Phe synthesis activity of cell lysates from WT or CNDP2-KO human cell lines U937 (C), Caco-2 (D), or PANC-1 (E). Bottom: western blot using an anti-CNDP2 (upper) or anti-tubulin (lower) antibody for WT and CNDP2-KO U937 (C), Caco-2 (D), and PANC-1 (E) cells.

(F and G) Levels of BHB-amino acids (F) or the indicated metabolite (G) in human plasma at baseline or 60 min post ketone ester drink administration (0.3 g/kg ketone ester).

For (A) and (C)–(E), reactions were performed with 20 mM substrates at 37°C for 1 h.

For (A)–(E), n = 3–5/group. For (F) and (G), n = 7/group. For (A)–(E), data are shown as mean ± SEM. For (F) and (G), data are shown as box-and-whisker pots. p values were calculated by Student's two-sided t test.

BHB, provided a compelling and directly testable biochemical hypothesis for the biosynthetic origins of BHB-amino acids. Second, our chemical synthesis of BHB-amino acid standards, which are otherwise not commercially available, enabled confirmation of the retention time and fragmentation of the endogenous peaks. Our strategy for detecting BHB-amino acids suggest that metabolome space might be more generally annotated by combining authentic metabolite standards with hypotheses about the chemical similarity of substrates and promiscuity of biochemical reactions.

Although our studies here only examined the role of BHB-amino acids in the context of energy homeostasis, the physiologic functions of BHB-amino acids may extend to other physiologic contexts as well. For instance, ketosis is being explored in a variety of other contexts, such as in neurodegenerative diseases,[26] inflammation,[27] muscle resilience,[28] cancer treatment,[29] and several other age-associated diseases. In addition, elevated BHB is observed in other pathophysiologic conditions, such as diabetic ketoacidosis. Our data demonstrate that BHB-amino acids are also produced when levels of BHB are high, raising the possibility that the effects of ketosis and BHB in these other contexts might also be, at least in part, mediated by concomitant production of BHB-amino acids.

Limitations of the study

There are four main limitations of this study. First, we show that BHB-Phe activates neural populations in the hypothalamus and brainstem. However, we do not further characterize the molecular identities of these neurons nor do we probe the functional consequences of their activation. In the future, such experiments would define which feeding-associated brain regions and cell types are important downstream effectors of the anorexigenic action of BHB-Phe. Second, our gain-of-function sufficiency studies with pharmacological administration of BHB-amino acids achieved supraphysiologic levels of metabolites in circulation. Although lower, more physiologically relevant concentrations were not tested here, such experiments may reveal more about the subtleties of how these ketone metabolites influence feeding and neural circuits in a physiological context. It is possible that lower, more physiologically relevant concentrations could selectively activate different subpopulations of neurons or produce more nuanced effects on feeding behavior or body weight. Such experiments might clarify the presence of potential dose-dependent "entourage effects," where combinations of BHB-amino acids act synergistically at lower doses to modulate neural or metabolic responses. Third, we have not yet identified CNDP2 point mutants that can only accept either BHB or lactate as substrates.

Such mutants would enable functional dissection of these multiple biochemical branches of CNDP2 activity *in vitro* and *in vivo*. Fourth, our study uses global CNDP2-KO mice, which does not enable specific assignment of cell types or tissues that contribute to total BHB-amino acid synthesis *in vivo*. The use of conditional CNDP2-KO mice might establish certain organs, such as the gut, which are more predominant contributors to whole-body BHB-amino acid synthesis.

RESOURCE AVAILABILITY

Lead contact

Further information and requests for resources and reagents should be directed to and will be fulfilled by the lead contact, Jonathan Long (jzlong@stanford.edu).

Materials availability

Chemical compounds generated in this study can be directly requested by email to the lead contact and are available without restrictions.

Data and code availability

- All data reported in this paper will be shared by the lead contact upon request.
- This paper does not report original code.
- Any additional information requested to re-analyze the data reported in this paper is available from the lead contact upon request.

ACKNOWLEDGMENTS

We thank members of the Long and Svensson laboratories for helpful discussions, Dr. Paul J. Emmerson (Eli Lilly & Co.) for sharing the anti-GFRAL neutralizing antibody, and the Centro de Supercomputación de la Universidad de Granada (CSIRC) for computing resources. This work was supported by the NIH (DK124265 and DK130541 to J.Z.L.; DK125260, DK111916, and P30DK116074 to K.J.S.; GM113854 to V.L.L.; HD112123 to M.W.; K99AR081618 to M.Z.; T32HL161270 to C.P.W.; R00AG058801 to E.L.G.; and T32GM136631 to A.S.-H.T.), the Phil & Penny Knight Initiative for Brain Resilience at the Wu Tsai Neurosciences Institute (research grant to J.Z.L.), the Ono Pharma Foundation (research grant to J.Z.L.), the Stanford Wu Tsai Human Performance Alliance (research grant to J.Z.L. and fellowship to X.L. and M.D.M.-G.), the Stanford Bio-X (SIGF graduate student fellowship to V.L.L.), the Jacob Churg Foundation (research grants to J.Z.L. and K.J.S.), the American Heart Association (fellowship #905674 to M.Z.), the Stanford School of Medicine (Dean's postdoctoral fellowship to L.C.), the Independent Research Fund Denmark (2030-00007A to S.H.R.), the Lundbeck Foundation (R380-2021-1451 to S.H.R.), the American Heart Association (24POST1196199 to W.W.), the CIHR (PJ9-166217 and PJT-169116 to J.P.L.), the Ovarian Cancer Research Alliance (MIG-2023-2-1015 to A.D.-G.), the Fundación Alfonso Martin Escudero (fellowship to M.D.M.-G. and A.D.-G.), and USDA/CRIS (51000-064-01S to Y.X.).

AUTHOR CONTRIBUTIONS

Conceptualization, M.D.M.-G. and J.Z.L.; investigation, M.D.M.-G., M.W., V.L.L., X.L., W.W., A.S.-H.T., S.H.R., L.C., M.Z., J.S., A.D.-G., K.D., A.A.-B., F.F.-M., and L.L.; writing – original draft, M.D.M.-G. and J.Z.L.; writing – review and editing, Y.X., J.Z.L., and M.D.M.-G.; resources, S.M.B., H.I., B.O., J.P.L., C.P.W., C.D.G., A.L., E.L.G., and Y.D.; supervision, J.Z.L., Y.X., S.M.B., and K.J.S.

DECLARATION OF INTERESTS

A provisional patent application has been filed by Stanford University on BHB-amino acids for the treatment of cardiometabolic disease.

STAR★METHODS

Detailed methods are provided in the online version of this paper and include the following:

- KEY RESOURCES TABLE
- EXPERIMENTAL MODEL AND STUDY PARTICIPANT DETAILS
  - Cell lines
  - Animals
  - Human subjects
- METHOD DETAILS
  - Chemicals
  - Synthesis of BHB-Phe
  - Synthesis of BHB-Val
  - Synthesis of BHB-Leu
  - Synthesis of BHB-Met
  - Synthesis of BHB-Lys
  - Synthesis of 2-HB amino acids
  - Synthesis of 3-HIB amino acids
  - Docking of BHB-Phe to CNDP2
  - CNDP2 mutagenesis
  - Recombinant mouse CNDP2 purification
  - *In vitro* kinetic assays with recombinant proteins
  - *In vitro* enzyme activity assays with cell lysates
  - Tissue enzyme activity assays
  - Generation of CNDP2-KO cells
  - Western blot analysis
  - Preparation of plasma and mouse tissues for LC-MS analysis
  - Targeted metabolomics
  - Breeding and genotyping of CNDP2-KO mice
  - Acute feeding and water intake assays
  - Indirect calorimetry
  - Leptin, ghrelin and GDF-15 measurements
  - Effect of GLP-1R antagonism on BHB-Phe-induced suppression of feeding
  - Effect of GFRAL antagonism on BHB-Phe-induced suppression of feeding
  - Effect of GDF-15 on body weight and food intake in mice injected with anti-GFRAL antibody
  - Sequential TRAP/c-Fos mapping BHB-Phe- and Lac-Phe-activated neurons in the brain
- QUANTIFICATION AND STATISTICAL ANALYSIS

SUPPLEMENTAL INFORMATION

Supplemental information can be found online at https://doi.org/10.1016/j.cell.2024.10.032.

Received: July 23, 2023
Revised: June 12, 2024
Accepted: October 16, 2024
Published: November 12, 2024

REFERENCES

1. Newman, J.C., and Verdin, E. (2017). β-hydroxybutyrate: A Signaling Metabolite. Annu. Rev. Nutr. *37*, 51–76.
2. Puchalska, P., and Crawford, P.A. (2021). Metabolic and signaling roles of ketone bodies in health and disease. Annu. Rev. Nutr. *41*, 49–77.
3. Rahman, M., Muhammad, S., Khan, M.A., Chen, H., Ridder, D.A., Müller-Fielitz, H., Pokorná, B., Vollbrandt, T., Stölting, I., Nadrowitz, R., et al. (2014). The b-hydroxybutyrate receptor HCA 2 activates a neuroprotective subset of macrophages. Nat. Commun. *5*, 1–11.
4. Kimura, I., Inoue, D., Maeda, T., Hara, T., Ichimura, A., Miyauchi, S., Kobayashi, M., Hirasawa, A., and Tsujimoto, G. (2011). Short-chain fatty acids and ketones directly regulate sympathetic nervous system via G

protein-coupled receptor 41 (GPR41). Proc. Natl. Acad. Sci. USA *108*, 8030–8035.

5. Xie, Z., Zhang, D., Chung, D., Tang, Z., Huang, H., Dai, L., Qi, S., Li, J., Colak, G., Chen, Y., et al. (2016). Metabolic regulation of gene expression by histone lysine β-Hydroxybutyrylation. Mol. Cell *62*, 194–206.
6. Shimazu, T., Hirschey, M.D., Newman, J., He, W., Shirakawa, K., Le Moan, N., Grueter, C.A., Lim, H., Saunders, L.R., Stevens, R.D., et al. (2013). Suppression of oxidative stress by beta-hydroxybutyrate, an endogenous histone deacetylase inhibitor. Science *339*, 211–214.
7. Goldberg, E.L., Letian, A., Dlugos, T., Leveau, C., and Dixit, V.D. (2023). Innate immune cell-intrinsic ketogenesis is dispensable for organismal metabolism and age-related inflammation. J. Biol. Chem. *299*, 103005.
8. Pierre, K., Parent, A., Jayet, P.Y., Halestrap, A.P., Scherrer, U., and Pellerin, L. (2007). Enhanced expression of three monocarboxylate transporter isoforms in the brain of obese mice. J. Physiol. *583*, 469–486.
9. Shafqat, N., Kavanagh, K.L., Sass, J.O., Christensen, E., Fukao, T., Lee, W.H., Oppermann, U., and Yue, W.W. (2013). A structural mapping of mutations causing succinyl-CoA:3-ketoacid CoA transferase (SCOT) deficiency. J. Inherit. Metab. Dis. *36*, 983–987.
10. Jansen, R.S., Addie, R., Merkx, R., Fish, A., Mahakena, S., Bleijerveld, O.B., Altelaar, M., IJlst, L., Wanders, R.J., Borst, P., et al. (2015). N-lactoyl-amino acids are ubiquitous metabolites that originate from CNDP2-mediated reverse proteolysis of lactate and amino acids. Proc. Natl. Acad. Sci. USA *112*, 6601–6606.
11. Li, V.L., He, Y., Contrepois, K., Liu, H., Kim, J.T., Wiggenhorn, A.L., Tanzo, J.T., Tung, A.S.H., Lyu, X., Zushin, P.H., et al. (2022). An exercise-inducible metabolite that suppresses feeding and obesity. Nature *606*, 785–790.
12. Xiao, S., Li, V.L., Lyu, X., Chen, X., Wei, W., Abbasi, F., Knowles, J.W., Tung, A.S.-H., Deng, S., Tiwari, G., et al. (2024). Lac-Phe mediates the effects of metformin on food intake and body weight. Nat. Metab. *6*, 659–669.
13. Scott, B., Day, E.A., O'Brien, K.L., Scanlan, J., Cromwell, G., Scannail, A.N., McDonnell, M.E., Finlay, D.K., and Lynch, L. (2024). Metformin and feeding increase levels of the appetite-suppressing metabolite Lac-Phe in humans. Nat. Metab. *6*, 651–658.
14. Smith, C.A., O'Maille, G., Want, E.J., Qin, C., Trauger, S.A., Brandon, T.R., Custodio, D.E., Abagyan, R., and Siuzdak, G. (2005). METLIN: a metabolite mass spectral database. Ther. Drug Monit. *27*, 747–751.
15. Wishart, D.S., Guo, A.C., Oler, E., Wang, F., Anjum, A., Peters, H., Dizon, R., Sayeeda, Z., Tian, S., Lee, B.L., et al. (2022). HMDB 5.0: the human metabolome database for 2022. Nucleic Acids Res. *50*, D622–D631.
16. Wang, M., Carver, J.J., Phelan, V.V., Sanchez, L.M., Garg, N., Peng, Y., Nguyen, D.D., Watrous, J., Kapono, C.A., Luzzatto-Knaan, T., et al. (2016). Sharing and community curation of mass spectrometry data with Global Natural Products Social Molecular Networking. Nat. Biotechnol. *34*, 828–837.
17. Gall, W.E., Beebe, K., Lawton, K.A., Adam, K.P., Mitchell, M.W., Nakhle, P.J., Ryals, J.A., Milburn, M.V., Nannipieri, M., Camastra, S., et al. (2010). A-hydroxybutyrate is an early biomarker of insulin resistance and glucose intolerance in a nondiabetic population. PLoS One *5*, e10883.
18. Nilsen, M.S., Jersin, R.Å., Ulvik, A., Madsen, A., McCann, A., Svensson, P.-A., Svensson, M.K., Nedrebø, B.G., Gudbrandsen, O.A., Tell, G.S., et al. (2020). 3-hydroxyisobutyrate, A strong marker of insulin resistance in type 2 diabetes and obesity that modulates white and brown adipocyte metabolism. Diabetes *69*, 1903–1916.
19. Emmerson, P.J., Wang, F., Du, Y., Liu, Q., Pickard, R.T., Gonciarz, M.D., Coskun, T., Hamang, M.J., Sindelar, D.K., Ballman, K.K., et al. (2017). The metabolic effects of GDF15 are mediated by the orphan receptor GFRAL. Nat. Med. *23*, 1215–1219.
20. Worth, A.A., Shoop, R., Tye, K., Feetham, C.H., D'agostino, G., Dodd, G.T., Reimann, F., Gribble, F.M., Beebe, E.C., Dunbar, J.D., et al. (2020). The cytokine GDF15 signals through a population of brainstem cholecystokinin neurons to mediate anorectic signalling. eLife *9*, 1–19.
21. DeNardo, L.A., Liu, C.D., Allen, W.E., Adams, E.L., Friedmann, D., Fu, L., Guenthner, C.J., Tessier-Lavigne, M., and Luo, L. (2019). Temporal evolution of cortical ensembles promoting remote memory retrieval. Nat. Neurosci. *22*, 460–469.
22. Falkenhain, K., Oliveira, B.F., Islam, H., Neudorf, H., Cen, H.H., Johnson, J.D., Madden, K., Singer, J., Walsh, J.J., and Little, J.P. (2024). The effect of acute and 14-day exogenous ketone supplementation on glycemic control in adults with type 2 diabetes: two randomized controlled trials. Am. J. Physiol. Endocrinol. Metab. *326*, E61–E72.
23. Nasser, S., Solé, T., Vega, N., Thomas, T., Balcerczyk, A., Strigini, M., and Pirola, L. (2022). Ketogenic diet administration to mice after a high-fat-diet regimen promotes weight loss, glycemic normalization and induces adaptations of ketogenic pathways in liver and kidney. Mol. Metab. *65*, 101578.
24. Laeger, T., Metges, C.C., and Kuhla, B. (2010). Role of β-hydroxybutyric acid in the central regulation of energy balance. Appetite *54*, 450–455.
25. Stubbs, B.J., Cox, P.J., Evans, R.D., Cyranka, M., Clarke, K., and de Wet, H. (2018). A ketone ester drink lowers human ghrelin and appetite. Obesity *26*, 269–273.
26. Fortier, M., Castellano, C.A., St-Pierre, V., Myette-Côté, É., Langlois, F., Roy, M., Morin, M.C., Bocti, C., Fulop, T., Godin, J.P., et al. (2021). A ketogenic drink improves cognition in mild cognitive impairment: results of a 6-month RCT. Alzheimers Dement. *17*, 543–552.
27. Youm, Y.H., Nguyen, K.Y., Grant, R.W., Goldberg, E.L., Bodogai, M., Kim, D., D'Agostino, D., Planavsky, N., Lupfer, C., Kanneganti, T.D., et al. (2015). The ketone metabolite β-hydroxybutyrate blocks NLRP3 inflammasome-mediated inflammatory disease. Nat. Med. *21*, 263–269.
28. Benjamin, D.I., Both, P., Benjamin, J.S., Nutter, C.W., Tan, J.H., Kang, J., Machado, L.A., Klein, J.D.D., de Morree, A., Kim, S., et al. (2022). Fasting induces a highly resilient deep quiescent state in muscle stem cells via ketone body signaling. Cell Metab. *34*, 902–918.e6.
29. Dmitrieva-Posocco, O., Wong, A.C., Lundgren, P., Golos, A.M., Descamps, H.C., Dohnalová, L., Cramer, Z., Tian, Y., Yueh, B., Eskiocak, O., et al. (2022). β-hydroxybutyrate suppresses colorectal cancer. Nature *605*, 160–165.
30. Unno, H., Yamashita, T., Ujita, S., Okumura, N., Otani, H., Okumura, A., Nagai, K., and Kusunoki, M. (2008). Structural basis for substrate recognition and hydrolysis by mouse carnosinase CN2. J. Biol. Chem. *283*, 27289–27299.
31. Morris, G.M., Huey, R., Lindstrom, W., Sanner, M.F., Belew, R.K., Goodsell, D.S., and Olson, A.J. (2009). Autodock4 and AutoDockTools4: automated docking with selective receptor flexiblity. J. Comput. Chem. *30*, 2785–2791.
32. Pettersen, E.F., Goddard, T.D., Huang, C.C., Couch, G.S., Greenblatt, D.M., Meng, E.C., and Ferrin, T.E. (2004). UCSF Chimera - A visualization system for exploratory research and analysis. J. Comput. Chem. *25*, 1605–1612.

STAR★METHODS

KEY RESOURCES TABLE

REAGENT or RESOURCE	SOURCE	IDENTIFIER
Antibodies		
Rabbit anti-CNDP2	Proteintech	14925-1-AP; RRID: AB_2081682
Anti-beta tubulin rabbit polyclonal	Abcam	Ab6046; RRID: AB_2210370
c-Fos (9F6) Rabbit mAb	Cell Signaling Technology	2250; RRID: AB_2247211
Donkey anti-Rabbit IgG (H+L) Highly Cross-Adsorbed Secondary Antibody, Alexa Fluor™ 488	Invitrogen	A21206; AB_2535792
Anti-GFRAL antibody and IgG control	Eli Lilly & Co.	Clone 8A2
Biological samples		
Human blood samples	Falkenhain et al.[22]	N/A
Chemicals, peptides, and recombinant proteins		
Sodium (*R*)-3-hydroxybutyrate	Sigma	298360
Sodium L-lactate	Sigma	L7022
Sodium octanoate	TCI Chemicals	O0034
Sodium acetate trihydrate	Mallinckrodt	7364
1-(3-Dimethylaminopropyl)-3-ethylcarbodiimide Hydrochloride	TCI Chemicals	D1601
1-hydroxybenzotriazole	TCI Chemicals	H0468-25G
N,*N*-diisopropylethylamine	Sigma	D125806
Dichloromethane	Sigma	270997
Lithium hydroxide	Sigma	442410-100G-A
L-Alanine	Sigma	A7627
L-Arginine	Sigma	A5006
L-Asparagine	Sigma	A0884
L-Aspartic acid	United States Biochemical Corporation	11625
L-Cysteine-HCl-H_2O	Thermo	44889
L-Glutamine	Sigma	G3126-100G
L-Glutamic acid monosodium salt monohydrate	Sigma	49621
Glycine	Fisher	G48-212
L-Histidine	Sigma	H8000
L-Isoleucine	Alfa Aesar	A13699
L-Leucine	Acros	12512-1000
L-Lysine	Sigma	L8662
L-Methionine	Sigma	M9625
L-Phenylalanine	Alfa Aesar	A13238
L-Proline	Sigma	P0380
L-Serine	Sigma	S2600
L-Threonine	Sigma	T8625
L-Tryptophan	Sigma	T0254
L-Tyrosine	Sigma	T8566-
L-Valine	Sigma	V0500
Ammonium acetate	Sigma	A2706

(*Continued on next page*)

Continued

REAGENT or RESOURCE	SOURCE	IDENTIFIER
Ammonium hydroxide	Fisher	A669-500
L-Phenylalanine ethyl ester hydrochloride	Sigma	220701
L-Methionine ethyl ester hydrochloride	Sigma	220671
L-Valine Ethyl Ester Hydrochloride	TCI Chemicals	V0142
L-Leucine ethyl ester hydrochloride	Fisher	AAL1314706
Sodium (*R,S*)-2-hydroxybutyrate	Alfa Aesar	A18636-03
Sodium (*R*)-3-hydroxyisobutyrate	Sigma	11161
Polyfect	Quiagen	301105
HALT protease inhibitor	Thermo Fisher	78429
Phe-Phe	Sigma	P4126-1G
Leu-Leu	Sigma	L2752-1G
Anti-FLAG M2 Magnetic Beads	Sigma	M8823
GLP-1 (7-37)	Genescript	RP12738-0.5
GDF-15	R&D systems	957-GD
CNDP2 Human Recombinant Protein	Origene	NM_018235
4-hydroxytamoxifen	Sigma	H6278
Exendin-3 (9-39) amide	Tocris	2081
DMSO	Sigma	472301
Kolliphor® EL	Sigma	C5135
Critical commercial assays		
Mouse Leptin ELISA Kit	Crystal Chem	90030
Acylated Ghrelin (mouse, rat) Express EIA Kit	Cayman Chemicals	10006307
Mouse GDF-15 DuoSet ELISA	R&D Systems	DY6385-05
Q5 Site-Directed Mutagenesis Kit	NEB	E0554S
Experimental models: Cell lines		
HEK 293T (*Homo-sapiens*)	ATCC	CRL-3216
Caco-2 (*Homo-sapiens*)	ATCC	HTB-37
U-937 (*Homo-sapiens*)	ATCC	CRL-1593.2
PANC-1 (*Homo-sapiens*)	ATCC	CRL-1469
Experimental models: Organisms/strains		
C57BL/6J (*M. musculus*)	Jackson Laboratory	000664
C57BL/6NCrl-Cndp2em1 (IMPC)Mbp/Mmucd (*M. musculus*)	Mutant Mouse Regional Resource Center	RRID: MMRRC_043492-UCD
MC4R-KO (*M. musculus*)	Jackson Laboratory	032518
C57BL/6NCrl mice (*M. musculus*)	Charles River Laboratory	027
Hmgcl$^{fl/fl}$ (*M. musculus*)	Pennington Biomedical Research Center Transgenics Core	N/A
Alb-cre (*M. musculus*)	Jackson Laboratory	003574
TRAP2 (*M. musculus*)	Jackson Laboratory	030323
Rosa26-LSL-tdTomato (*M. musculus*)	Jackson Laboratory	007905
Oligonucleotides		
CNDP2 WT genotyping 5'-CAGATGGCTCGGA GATACCAC-3';	Elim Biopharm	N/A
CNDP2 WT genotyping 5'-TTCCCGCTCCACC AAGGTGAAG-3'	Elim Biopharm	N/A
CNDP2 KO genotyping 5'-GCTCTGTAAGGG AAAGAGATGACCC-3';	Elim Biopharm	N/A

(*Continued on next page*)

Continued

REAGENT or RESOURCE	SOURCE	IDENTIFIER
CNDP2 KO genotyping 5'-AATAGGACATAC CCAGTTCTGTGAGG-3'	Elim Biopharm	N/A
CNDP2 E166D mutagenesis, primer 1: GGAAGGCATGgatGAGTCTGGCT	Elim Biopharm	N/A
CNDP2 E166D mutagenesis, primer 2: AGGCAGAACCGCAGG	Elim Biopharm	N/A
CNDP2 E166L mutagenesis, primer 1: GGAAGGCATGctgGAGTCTGGCTC	Elim Biopharm	N/A
CNDP2 E166L mutagenesis, primer 2: AGGCAGAACCGCAGG	Elim Biopharm	N/A
CNDP2 D195A mutagenesis, primer 1: GTGCATTTCAgcgAATTACTGGC	Elim Biopharm	N/A
CNDP2 D195A mutagenesis, primer 2: ACATAGTCCACATCTTTG	Elim Biopharm	N/A
CNDP2 H445F mutagenesis, primer 1: TGACGGTGCCtttTCGCAGAATGAG	Elim Biopharm	N/A
CNDP2 H445F mutagenesis, primer 2: TCTGCTGACCCCACTG	Elim Biopharm	N/A
Recombinant DNA		
mCNDP2 cDNA, C-term myc-DDK tagged plasmid	Origene	MR207616
mCNDP2 Mutant, E166D plasmid	This paper	N/A
mCNDP2 Mutant, E166L plasmid	This paper	N/A
mCNDP2 Mutant, D195A plasmid	This paper	N/A
mCNDP2 Mutant, H445F plasmid	This paper	N/A
Software and algorithms		
Prism 10.2.3	Graphpad	https://www.graphpad.com/
ChemDraw Professional 18	Revvity Signals	https://revvitysignals.com/products/research/chemdraw
Autodock 4.2.6	Morris et al.[31]	https://autodock.scripps.edu/download-autodock4/
UCSF Chimera 1.15	Pettersen et al.[32]	https://www.cgl.ucsf.edu/chimera/download.html
Other		
Heparin tubes	BD	365985
EDTA tubes	BD	367863
GoTaq® Master Mixes	Promega	M7122
NH_2 100 Å LC column	Phenomenex	00B-4378-E0
Teklad 2018	Inotiv	N/A
High-fat diet with 60 kcal% fat	Research diets	D12492
Ketogenic diet (80% kcal fat, 15% kcal protein, 5% kcal carbohydrate)	Research diets	D06040601
Ketogenic diet (89% of calories from fat, 10% of calories from protein, 1% of calories from carbohydrates)	Research diets	D21021803
Delta G Tactical Ketones	Delta G Ketones	N/A
Pierce BCA Protein Assay Kit	Thermo Fisher	23225
Pico Lab diet	LabDiet	5V5R

EXPERIMENTAL MODEL AND STUDY PARTICIPANT DETAILS

Cell lines

All cell lines were obtained from ATCC and grown at 37°C with 5% CO_2. U-937 cells were a gift from Garry. P. Nolan. HEK293T, Caco-2 and PANC-1 cells were grown in Dulbecco's modified Eagle's medium (DMEM) with 10% fetal bovine serum (FBS) and

penicillin/streptomycin (pen/strep). U-937 cells were grown in RPMI-1640 medium with 10% fetal bovine serum (FBS) and penicillin/streptomycin (pen/strep). All cell lines were used directly from ATCC vials and were not specifically authenticated for this study. Cell lines were negative upon testing for mycoplasma contamination.

Animals

Animal experiments were performed according to procedure approved by the Stanford University Administrative Panel on Laboratory Animal Care (APLAC) or the Baylor College of Medicine Institutional Animal Care and Use Committees. Mice were maintained in 12-hr light-dark cycles at 22 °C and ~50% relative humidity and fed a standard irradiated rodent chow diet (Teklad 2018, Inotiv, Stanford; or Pico Lab, LabDiet, 5V5R, Baylor). Where indicated, high-fat diet (D12492, Research Diets 60% kcal from fat) and ketogenic diet (Research Diets D06040601 or D21021803) was used. Male C57BL/6J (stock no. 000664), male C57BL/6J DIO (stock no. 380050), male MC4R-KO (stock no. 032518), male TRAP2 (stock no. 030323), female Rsa26-LSL-tdTomato (stock no. 007905) mice, and male Albumin-cre (stock no. 003574) were purchased from Jackson Laboratory. Male C57BL/6NCrl (stock no. 027) mice were purchased from Charles River Laboratory. Heterozygous CNDP2 mice (catalog number, C57BL/6NCrl-Cndp2e-m1(IMPC)Mbp/Mmucd, RRID: MMRRC_043492-UCD) were obtained from the Mutant Mouse Regional Resource Center, a NCRR-NIH funded strain repository. TRAP2/Rosa26-LSL-tdTomato mice were generated by crossing TRAP2 mice with Rsa26-LSL-tdTomato mice. CNDP2-KO mice and WT littermate controls were generated from heterozygous breeding crosses. The genotype, age, and sex of mice used in experiments are reported directly in the figure legends. For *in vivo* injection of mice with metabolites, compounds were dissolved in 18:1:1 (by volume) of saline/Kolliphor EL (Sigma Aldrich)/DMSO and were administered to mice via intraperitoneal injections at 5 μl/g body weight at the indicated doses. For injection and oral gavage experiments measuring food intake and body weight, mice were singly housed unless otherwise specified. Mice were mock injected with the vehicle for 3-5 days until body weights were stabilized. All procedures were performed around 18:00. For studies in DIO mice, initial baseline body weights ranged between 35-45g, were matched between vehicle and treatment groups to within 2 g, and were not different between groups. Ketone ester drink oral gavage to mice was performed using ΔG Tactical Ketones. The ketone ester drink was diluted 1:1 (by volume) in drinking water and 5.6 μl/g body weight were administered to mice by oral gavage. Sample sizes were determined based on previous experiments using similar methodologies. For metabolite administration experiments, mice were randomly assigned to treatment groups. For experiments involving WT and CNDP2-KO mice, littermates of the same sex were randomly assigned to experimental groups. Experimenters were not blinded to groups.

Human subjects

The human exogenous ketone supplementation study was previously reported.[22] Procedures for this study were followed in accordance with the ethical standards from the Helsinki Declaration and were approved by the University of British Columbia Clinical Research Ethics Board (CREB). Of those study participants, the first 7 individuals (3 females) with complete blood samples in the ketone monoester condition were included for mass spectrometry analyses of BHB-amino acids (age: 65.4±4.4 years, body mass index: 28.4±5.0 kg/m^2, waist circumference: 101.7±17.2 cm, HbA1c: 7.1±0.5%, blood pressure: 134/77±10/13 mmHg). Six participants were White/Caucasian and one participant was Southeast Asian. Blinding was maintained until completion of data collection and analyses.

METHOD DETAILS

Chemicals

The full inventory of commercially available compounds, purchased from Fisher, Sigma, Alfa Aesar, TCI, Mallinckrodt, United States Biochemical Corporation, Thermo, and Acros, is described in key resources table. The synthesis of BHB-amino acids, 2-HB-amino acids, and 3-HIB-amino acids are described below. ^{1}H NMR spectra for new compounds can be found in Data S1. The GFRAL neutralizing antibody (clone 8A2) and control IgG antibody were obtained from Eli Lilly & Co. (P. J. Emmerson).

Synthesis of BHB-Phe

1-ethyl-3-(3-dimethylaminopropyl)carbodiimide (1.05 eq.) was added to a cold mixture of (*R*)-3-hydroxybutyrate (1 eq.) and 1-hydroxybenzotriazole (1 eq.) in dichloromethane (0.2 M) under argon. After 10 min, L-phenylalanine ethyl ester hydrochloride (1 eq.) and *N*,*N*-diisopropylethylamine (3 eq.) in dichloromethane (0.2 M) were added to the mixture. The ice bath was removed and the reaction was stirred for 16 h under argon at ambient temperature. One-third of the solvent was then removed and the dichloromethane solution was washed with 5% HCl, 5% $NaHCO_3$ and saturated NaCl solutions. The organic layer was dried over $MgSO_4$, filtered and concentrated. The resulting crude product was purified by column chromatography, eluting with ethyl acetate/hexane to afford the *N*-β-hydroxybutyryl phenylalanine ethyl ester. The above ester was dissolved in tetrahydrofuran (0.5 M) and 2 N LiOH (2 eq.) was added. The resulting mixture was stirred at room temperature for 2 h. The solvent was then removed and the resulting residue was dissolved in water and acidified with 5% HCl to pH 3. The resulting mixture was extracted with ethyl acetate three times, and the combined organic layers were washed with saturated NaCl solution. The organic layer was dried over $MgSO_4$, filtered, concentrated, coevaporated three times with DCM and then dried under high vacuum to give BHB-Phe (*N*-β-hydroxybutyryl-phenylalanine) as a white powder. ^{1}H NMR (400 MHz, Methanol-d$_4$): δ 7.23 (dq, *J* = 16.1, 8.6, 7.9 Hz, 5H), 4.66 (dd, *J* = 8.5,

5.2 Hz, 1H), 4.01 (dt, *J* = 12.5, 6.2 Hz, 1H), 3.19 (dd, J = 13.9, 5.1 Hz, 1H), 2.95 (dd, *J* = 13.9, 8.8 Hz, 1H), 2.28 (qd, *J* = 14.2, 6.5 Hz, 2H), 1.16 – 1.06 (m, 3H). MS (*m/z*): 250.108 $[M–H]^-$.

Synthesis of BHB-Val

1-ethyl-3-(3-dimethylaminopropyl)carbodiimide (1.05 eq.) was added to a cold mixture of sodium (*R*)-3-hydroxybutyrate (1 eq.) and 1-hydroxybenzotriazole (1 eq.) in dichloromethane (0.2 M) under argon. After 10 min, L-valine ethyl ester hydrochloride (1 eq.) and *N*,*N*-diisopropylethylamine (3 eq.) in dichloromethane (0.2 M) were added to the mixture. The ice bath was removed and the reaction was stirred for 16 h under argon at ambient temperature. One-third of the solvent was then removed and the dichloromethane solution was washed with 5% HCl, 5% $NaHCO_3$ and saturated NaCl solutions. The organic layer was dried over $MgSO_4$, filtered and concentrated. The resulting crude product was purified by column chromatography, eluting with ethyl acetate/hexane to afford the *N*-β-hydroxybutyryl valine ethyl ester. The above ester was dissolved in tetrahydrofuran (0.5 M) and 2 N LiOH (2 eq.) was added. The resulting mixture was stirred at room temperature for 2 h. The solvent was then removed and the resulting residue was dissolved in water and acidified with 5% HCl to pH 3. The resulting mixture was extracted with ethyl acetate three times, and the combined organic layers were washed with saturated NaCl solution. The organic layer was dried over $MgSO_4$, filtered, concentrated, coevaporated three times with DCM and then dried under high vacuum to give BHB-Val (*N*-β-hydroxybutyryl-valine) as a colorless syrup. ^{1}H NMR (400 MHz, Methanol-d_4): δ 4.29 (d, *J* = 5.3 Hz, 1H), 4.09 (dq, *J* = 12.4, 6.1 Hz, 1H), 2.35 (qt, *J* = 14.2, 6.5 Hz, 2H), 2.12 (dq, *J* = 13.5, 6.8 Hz, 1H), 1.17 (d, *J* = 6.2 Hz, 3H), 1.00 – 0.86 (m, 6H). MS (*m/z*): 202.108 $[M–H]^-$.

Synthesis of BHB-Leu

1-ethyl-3-(3-dimethylaminopropyl)carbodiimide (1.05 eq.) was added to a cold mixture of sodium (*R*)-3-hydroxybutyrate (1 eq.) and 1-hydroxybenzotriazole (1 eq.) in dichloromethane (0.2 M) under argon. After 10 min, L-leucine ethyl ester hydrochloride (1 eq.) and *N*,*N*-diisopropylethylamine (3 eq.) in dichloromethane (0.2 M) were added to the mixture. The ice bath was removed and the reaction was stirred for 16 h under argon at ambient temperature. One-third of the solvent was then removed and the dichloromethane solution was washed with 5% HCl, 5% $NaHCO_3$ and saturated NaCl solutions. The organic layer was dried over $MgSO_4$, filtered and concentrated. The resulting crude product was purified by column chromatography, eluting with ethyl acetate/hexane to afford the *N*-β-hydroxybutyryl leucine ethyl ester. The above ester was dissolved in tetrahydrofuran (0.5 M) and 2 N LiOH (2 eq.) was added. The resulting mixture was stirred at room temperature for 2 h. The solvent was then removed and the resulting residue was dissolved in water and acidified with 5% HCl to pH 3. The resulting mixture was extracted with ethyl acetate three times, and the combined organic layers were washed with saturated NaCl solution. The organic layer was dried over $MgSO_4$, filtered, concentrated, coevaporated three times with DCM and then dried under high vacuum to give BHB-Leu (*N*-β-hydroxybutyryl-leucine) as a colorless syrup. ^{1}H NMR (400 MHz, Methanol-d_4): ^{1}H NMR (400 MHz, Methanol-d4) δ 4.47 – 4.39 (m, 1H), 4.19 – 4.08 (m, 1H), 2.43 – 2.29 (m, 2H), 1.73 (dp, *J* = 13.0, 6.5 Hz, 1H), 1.67 – 1.58 (m, 2H), 1.21 (d, *J* = 6.2 Hz, 3H), 0.95 (dd, *J* = 13.6, 6.5 Hz, 6H). MS (*m/z*): 216.124 $[M–H]^-$.

Synthesis of BHB-Met

1-ethyl-3-(3-dimethylaminopropyl)carbodiimide (1.05 eq.) was added to a cold mixture of sodium (*R*)-3-hydroxybutyrate (1 eq.) and 1-hydroxybenzotriazole (1 eq.) in dichloromethane (0.2 M) under argon. After 10 min, L-methionine ethyl ester hydrochloride (1 eq.) and *N*,*N*-diisopropylethylamine (3 eq.) in dichloromethane (0.2 M) were added to the mixture. The ice bath was removed and the reaction was stirred for 16 h under argon at ambient temperature. One-third of the solvent was then removed and the dichloromethane solution was washed with 5% HCl, 5% $NaHCO_3$ and saturated NaCl solutions. The organic layer was dried over $MgSO_4$, filtered and concentrated. The resulting crude product was purified by column chromatography, eluting with ethyl acetate/hexane to afford the *N*-β-hydroxybutyryl methionine ethyl ester. The above ester was dissolved in tetrahydrofuran (0.5 M) and 2 N LiOH (2 eq.) was added. The resulting mixture was stirred at room temperature for 2 h. The solvent was then removed and the resulting residue was dissolved in water and acidified with 5% HCl to pH 3. The resulting mixture was extracted with ethyl acetate three times, and the combined organic layers were washed with saturated NaCl solution. The organic layer was dried over $MgSO_4$, filtered, concentrated, coevaporated three times with DCM and then dried under high vacuum to give BHB-Met (*N*-β-hydroxybutyryl-methionine) as a white powder. ^{1}H NMR (400 MHz, Methanol-d_4): δ 4.62 – 4.45 (m, 1H), 4.12 (d, *J* = 8.6 Hz, 1H), 2.66 – 2.44 (m, 2H), 2.45 – 2.24 (m, 2H), 2.23 – 1.81 (m, 5H), 1.28 – 1.08 (m, 3H). MS (*m/z*): 234.0801 $[M–H]^-$.

Synthesis of BHB-Lys

To a solution of (*R*)-3-((tert-butyldiphenylsilyl)oxy)butanoic acid (4.0 g, 11.7 mmol, 1.0 eq) in dimethylformamide (90 mL) at 0°C were added *O*-[*N*-succinimidyl)-1,1,3,3-tetramethyluronium tetrafluoroborate (TSTU, 3.9 g, 12.9 mmol, 1.1 eq) and *N*,*N*-Diisopropylethylamine (DIEA, 7.5 g, 58.5 mmol, 5.0 eq). The reaction mixture was stirred at ambient temperature for 2 h. Then N^6-(tert-butoxycarbonyl)-L-lysine (3.2 g, 12.9 mmol, 1.1 eq) was added and the reaction mixture was stirred at ambient temperature for 16 h. The mixture was concentrated. The residue was diluted with water (100 mL) and extracted with ethyl acetate (100 mL x 3). The organic layer was dried over anhydrous Na_2SO_4, filtered and concentrated. The residue was purified by silica gel column chromatography (DCM/MeOH = 10/1) to afford compound N^6-(tert-butoxycarbonyl)-N^2-((R)-3-((tert-butyldiphenylsilyl)oxy)butanoyl)-L-lysine as white solid. To a solution of compound N^6-(tert-butoxycarbonyl)-N^2-((*R*)-3-((tert-butyldiphenylsilyl)oxy)butanoyl)-L-lysine (2.4 g, 4.2 mmol, 1.0 eq) in dioxane (10 mL) was added HCl/dioxane (20 mL, 4 M) and stirred at rt for 16 h. Once LCMS showed

N^6-(tert-butoxycarbonyl)-N^2-((R)-3-((tert-butyldiphenylsilyl)oxy)butanoyl)-L-lysine was consumed completely, the reaction mixture was concentrated. The residue was purified by prep-HPLC (0.1% HCOOH CH_3CN/water, 0-10%) to afford BHB-Lys (*N*-β-hydroxybutyryl-lysine) as white solid. ^{1}H NMR (400 MHz, D_2O) δ 4.35 – 4.32 (m, 1H), 4.21 – 4.13 (m, 1H), 2.99 – 2.95 (m, 2H), 2.45 – 2.40 (m, 2H), 1.89 – 1.83 (m, 1H), 1.77 – 1.63 (m, 3H), 1.46 – 1.40 (m, 2H), 1.21 (d, J = 6.4 Hz, 3H). MS (*m/z*): 234.080 $[M+H]^+$.

Synthesis of 2-HB amino acids

1-ethyl-3-(3-dimethylaminopropyl)carbodiimide (1.05 eq.) was added to a cold mixture of (*R,S*)-2-hydroxybutyrate (1 eq.) and 1-hydroxybenzotriazole (1 eq.) in dichloromethane (0.2 M) under argon. After 10 min, the corresponding ethyl ester hydrochloride for each amino acid (1 eq.) and *N*,*N*-diisopropylethylamine (3 eq.) in dichloromethane (0.2 M) were added to the mixture. The ice bath was removed and the reaction was stirred for 16 h under argon at ambient temperature. One-third of the solvent was then removed and the dichloromethane solution was washed with 5% HCl, 5% $NaHCO_3$ and saturated NaCl solutions. The organic layer was dried over $MgSO_4$, filtered and concentrated. The resulting crude product was directly dissolved in tetrahydrofuran (0.5 M) and 2 N LiOH (2 eq.) was added. The resulting mixture was stirred at room temperature for 2 h. The solvent was then removed and the resulting residue was dissolved in water and acidified with 5% HCl to pH 3. The resulting mixture was extracted with ethyl acetate three times, and the combined organic layers were washed with saturated NaCl solution. The organic layer was dried over $MgSO_4$, filtered, concentrated to give the corresponding 2-HB amino acid as a colorless syrup. The resulting crude product was used directly analyzed by LC-MS/MS.

Synthesis of 3-HIB amino acids

1-ethyl-3-(3-dimethylaminopropyl)carbodiimide (1.05 eq.) was added to a cold mixture of (*R*)-3-hydroxyisobutyrate (1 eq.) and 1-hydroxybenzotriazole (1 eq.) in dichloromethane (0.2 M) under argon. After 10 min, the corresponding ethyl ester hydrochloride for each amino acid (1 eq.) and *N*,*N*-diisopropylethylamine (3 eq.) in dichloromethane (0.2 M) were added to the mixture. The ice bath was removed and the reaction was stirred for 16 h under argon at ambient temperature. One-third of the solvent was then removed and the dichloromethane solution was washed with 5% HCl, 5% $NaHCO_3$ and saturated NaCl solutions. The organic layer was dried over $MgSO_4$, filtered and concentrated. The resulting crude product was directly dissolved in tetrahydrofuran (0.5 M) and 2 N LiOH (2 eq.) was added. The resulting mixture was stirred at room temperature for 2 h. The solvent was then removed and the resulting residue was dissolved in water and acidified with 5% HCl to pH 3. The resulting mixture was extracted with ethyl acetate three times, and the combined organic layers were washed with saturated NaCl solution. The organic layer was dried over $MgSO_4$, filtered, concentrated to give the corresponding 3-HIB amino acid as a colorless syrup. The resulting crude product was used directly analyzed by LC-MS/MS.

Docking of BHB-Phe to CNDP2

Pdb ID 2ZOF, an X-ray crystal structure of murine cytosolic non-specific dipeptidase 2 (CNDP2), was selected for docking analysis. To date, 2ZOF is the only published X-ray crystal structure of murine CNDP2 with two Mn^{2+} atoms on its active center.[30] It is an homodimer containing two active sites, each of which has one bestatin molecule, a nonhydrolyzable substrate analog inhibitor, and two Mn^{2+}. The complete homodimer structure was used for the docking studies on Autodock 4.2.6 software (AD4).[31] Ligands structures were built on Avogadro and optimized using Gaussian (HF/6-31G(d,p)). Once optimized, ligands PDBs were prepared for docking using the prepare_ligand4.py script included MGLTools 1.5.4. Protein structure, was energy minimized with using Swiss-PdbViewer default parameters with GROMOS96 43B1 forcefield, and prepared for docking using the DockPrep module in UCSF Chimera 1.15.[32] Ligand molecules were removed, and charges and non-polar hydrogen atoms were added. The produced structures were saved as a pdb files and prepared for docking using the prepare_receptor4.py script from MGLTools. The Mn atoms were assigned a charge of +2. AD4 was used to automatically dock the ligands into the active site of subunit A. The docking grid was centered on the cognate ligand (bestatin, BES) binding site and set with the following grid parameters: 60 Å × 60 Å × 60 Å with 0.375 Å spacing. In all calculations, AD4 parameter file was set to 100 GA runs, 2.500.000 energy evaluations and a population size of 150. The Lamarckian genetic algorithm local search (GALS) method was used for the docking calculations. All dockings were performed with a population size of 250 and a Solis and Wets local search of 300 rounds was applied with a probability of 0.06. A mutation rate of 0.02 and a crossover rate of 0.8 were used. The docking results from each of the 100 calculations were clustered based on root-mean square deviation (RMSD) solutions differing by less than 2.0 Å between the Cartesian coordinates of the atoms and ranked on the basis of free energy of binding. The obtained conformations were individually inspected using UCSF Chimera 1.15. This software was also used for figures generation.

CNDP2 mutagenesis

A Q5 Site-Directed Mutagenesis Kit was used to introduce mutations in amino acid residues predicted to be involved in the Mn^{2+} atoms stabilization and establishing interactions with BHB-Phe. The mutations introduced were verified through plasmid sequencing conducted by Genewiz.

Recombinant mouse CNDP2 purification

HEK293T cells were seeded in 15 cm plates at 11 million cells per plate and the next day transfected using polyfect with 27 μg of FLAG tagged mouse CNDP2. Cells were refreshed with new media the next day, and the day after collected for FLAG pulldown. On the day of collection, cells were washed 2 times with PBS and centrifuged to obtain the cell pellet. The pellet was re-suspended in PBS and sonicated. The whole cell lysate was then centrifuged for 30 minutes at 15,000 rpm at 4 °C to separate the membrane pellet and cytosolic supernatant. FLAG beads were washed 3 times with PBS and then incubated with the cell supernatant overnight at 4 °C on rotation. After overnight incubation, the beads were washed 3 times with PBS before eluting with 0.1 mg/ml FLAG peptide in PBS (kept on rotation for 1 hour at room temperature). The concentration of recombinant CNDP2 was calculating using a FLAG blot with a protein standard curve.

In vitro kinetic assays with recombinant proteins

The in vitro reactions were conducted in Eppendorf tubes with recombinant purified mouse CNDP2-FLAG protein (1 μg/reaction) or recombinant human CNDP2 (50 ng/reaction) with 20 mM phenylalanine and the indicated increasing concentrations of BHB or lactate. Reactions were incubated for 1 h at 37°C and 10 μl of 1 M HCl were added to acidify the medium and to protonate BHB-amino acids. Reactions were vortexed and 400 μl of ethyl acetate were added to each reaction. Reactions were vortexed for 30 s to extract BHB-Phe and Lac-Phe into the organic layer and centrifuged at 4 °C for 10 min at 15,000 r.p.m. A total of 300 μl from the top layer was transferred to a new Eppendorf tube and dried down under a stream of nitrogen. The residue was re-suspended in 100 μl of an 2:1:1 mixture of acetonitrile:methanol:water. The mixture was centrifuged at 4 °C for 10 min at 15,000 r.p.m. and the supernatant was transferred to a LC–MS vial.

In vitro enzyme activity assays with cell lysates

HEK293T cells were transfected with GFP, CNDP2 or CNDP2 mutants using PolyFect (Qiagen 301105) according to the manufacturer's instructions. The medium was changed one day post-transfection. After an additional 24 h, the cells were harvested in PBS, lysed by sonication and centrifuged (10 min at 15,000 rpm) to remove debris. Supernatant was collected and protein concentrations were adjusted. The in vitro reactions were conducted in Eppendorf tubes with 100 μl of 1 mg/mL protein and 20 mM substrates. Reactions were incubated for 1 h at 37°C and 10 μl of 1 M HCl were added to acidify the medium and to protonate BHB-amino acids. Reactions were vortexed and 400 μl of ethyl acetate were added to each reaction. Reactions were vortexed for 30 s to extract BHB-amino acids into the organic layer and centrifuged at 4 °C for 10 min at 15,000 r.p.m. A total of 300 μl from the top layer was transferred to a new Eppendorf tube and dried down under a stream of nitrogen. The residue was re-suspended in 150 μl of an 2:1:1 mixture of acetonitrile:methanol:water. The mixture was centrifuged at 4 °C for 10 min at 15,000 r.p.m. and the supernatant was transferred to a LC–MS vial.

Tissue enzyme activity assays

Mouse tissues were mixed with cold PBS and homogenized using a Benchmark BeadBlaster Homogenizer at 4 °C. Protein concentrations were adjusted using a BCA Protein Assay Kit and the resulting crude was filtered through a 0.45-μm filter to remove insoluble materials. The in vitro reactions were conducted in Eppendorf tubes with 200 μg protein and incubation with the corresponding substrates at 37°C for 1 hour. After that time, 10 μl of HCl and 400 μl of ethyl acetate were added in the BHB and lactate reactions and the samples were vortexed for 30 s. Reactions were centrifuged at 4 °C for 10 min at 15,000 r.p.m. and a total of 300 μl from the top layer was transferred to a new Eppendorf tube and dried down under a stream of nitrogen. The residue was re-suspended in 100 μl of an 2:1:1 mixture of acetonitrile:methanol:water. The mixture was centrifuged at 4 °C for 10 min at 15,000 r.p.m. and the supernatant was transferred to a LC–MS vial. For carnosine reactions, the reactions were not acidified and were directly quenched with 300 μl of an 2:1:1 mixture of acetonitrile:methanol:water after the 1 h incubation and vortexed for 30 s. The mixture was centrifuged at 4 °C for 10 min at 15,000 r.p.m. and the supernatant was transferred to a LC–MS vial.

Generation of CNDP2-KO cells

CNDP2-KO Caco-2 cells have been previously reported.[12] For U-937 and PANC1 cells, the sgRNA used was 5′-CAGGTGCCCG TAAATGCACA-3′. The following oligonucleotides were used to clone the sgRNA into the plentiCRISPRv2 vector: forward, 5′-CACC CAGGTGCCCGTAAATGCACA-3′; reverse, 5′-AAACTGTGCATTTACGGGCACCTGC-3′. Lentivirus particles were generated in the HEK293T cell line using Polyfect for the co-transfection of the cloned plentiCRISPRv2 plasmid with the viral packing psPAX2 plasmid and the viral envelope pMD2.G plasmid. A parental plentiCRISPRv2 plasmid was used as a control. Lentiviral supernatants were collected after 24 h and filtered through a 0.45-μM filter. The supernatant was then mixed in a 1:1 ratio with polybrene to a final concentration of 8 μg/ml polybrene. This mixture was added to cells at 40–50% confluence in 6-well plates. Transduced cells were transferred to a 10-cm plate followed by selection by puromycin for 3–6 days.

Western blot analysis

Cells were collected and lysed by sonication in RIPA buffer containing 1:100 HALT protease inhibitor. Cell lysates were centrifuged at 4 °C for 10 minutes at 13,000 rpm to remove residual cell debris. Protein concentrations of the supernatant were normalized using the Pierce BCA protein assay kit and combined with 4 x NuPAGE LDS Sample Buffer with 10 mM DTT. Samples were then boiled for

10 minutes at 95 °C. Tissues were dissected, collected into Eppendorf tubes, and immediately frozen with liquid nitrogen. Tissues were mixed with 0.5 ml cold RIPA buffer and homogenized using a Benchmark BeadBlaster homogenizer at 4°C. The homogenate was centrifuged at 13,000 r.p.m. for 10 min at 4°C to pellet insoluble materials. The supernatant was quantified using the BCA protein Assay Kit. Prepared samples were run on a NuPAGE 4-12% Bis-Tris gel then transferred to nitrocellulose membranes. Blots were blocked for 30 minutes at room temperature in Odyssey blocking buffer. Primary antibodies (rabbit anti-CNDP2 and rabbit anti-Beta-Tubulin) were added to Odyssey blocking buffer at a ratio of 1:1000. Blots were incubated in the indicated primary antibodies overnight while shaking at 4 °C. The following day, blots were washed 3 times with PBS-T, 10 minutes each before staining with the secondary antibody for 1 hour at room temperature. The secondary antibody used was a goat anti-rabbit antibody diluted in blocking buffer to a ratio of 1:10,000. Following secondary antibody staining, the blot was washed 3 times with PBS-T before being imaged with the Odyssey CLx Imaging System.

Preparation of plasma and mouse tissues for LC-MS analysis

Blood was collected from mice via a submandibular bleed into lithium heparin tubes and immediately transferred onto ice. Blood was centrifuged at 4 °C at 5,000 rpm for 5 min and the top layer of plasma was aliquoted and frozen at -80 °C. To extract polar metabolites from plasma for LC-MS analysis, 150 μl of a 2:1 mixture of acetonitrile/methanol was added to 50 μl of plasma. The mixture was centrifuged at 4 °C for 10 min at 15,000 rpm and the supernatant was transferred to a LC-MS vial. For the rest of tissues, tissues were homogenized in water at 250 mg/ml using a Benchmark BeadBlaster Homogenizer at 4 °C. The mixture was centrifuged at 4 °C for 10 min at 15,000 rpm to pellet insoluble materials and the supernatant was collected. To extract polar metabolites from tissues for LC-MS analysis, 150 ul of a 2:1 mixture of acetonitrile/Methanol was added to 50 μl of tissue homogenate. The mixture was centrifuged at 4 °C for 10 min at 15,000 rpm and the supernatant was transferred to a LC-MS vial.

Targeted metabolomics

The MS ionization parameters for the targeted metabolomics are presented in Table S1. Targeted measurements were performed using an Agilent 6470 triple quadrupole LC-MS instrument. MS analysis was performed using AJS in negative mode. The AJS source parameters were set as follows: the dry gas temperature was set at 250 °C with a gas flow of 12 l/min and the nebulizer pressure at 25 psi; the sheath gas temperature was set to 300 °C with the sheath gas flow set at 12 l/min; and the capillary voltage was set to 3,500 V. Separation of polar metabolites was conducted using a Luna 5 μm NH_2 100 Å LC column (Phenomenex 00G-4378-E0) with normal phase chromatography. Mobile phases were as follows: Buffer A, acetonitrile; Buffer B, 95:5 water/acetonitrile with 0.2% ammonium hydroxide and 50 mM ammonium acetate for negative ionization mode. The flow rate for each run started 100% B for 2 minutes at 0.7 ml/min, followed by a gradient starting at 100% B changing linearly to 50% A / 50% B over the course of 18 minutes at 0.7 ml/min, followed by 50% A / 50% B for 5 minutes at 0.7 ml/min. The last 5 minutes consisted of re-equilibration at 100% B prior to the next run. Multiple reaction monitoring was performed for the indicated metabolites with the listed dwell times, fragmentor voltage, collision energies, cell accelerator voltages and polarities. Quantification of the endogenous metabolite concentrations were performed by generating an external standard curve with known concentrations of each metabolite. Metabolite standards were analyzed alongside the plasma samples using the same targeted triple quadrupole LC/MS method in the same run. A calibration standard curve generated from the metabolite standard concentrations and total peak areas were used to calculate the concentrations of each endogenous metabolite.

Breeding and genotyping of CNDP2-KO mice

CNDP2 heterozygous mice were obtained from the International Mouse Genotyping Consortium (IMPC). CNDP2-KO and WT littermates were generated via heterozygous breeding crosses and age-matching was done to the extent possible given litter sizes and variation in genotypes. Genotyping was performed as follows: Tail clippings were obtained from littermates and boiled for 30 minutes at 95 °C in 100 μl of 50 mM NaOH to extract genomic DNA. The solution was neutralized by adding 21 μl of 0.5 M Tris (pH 7.2). PCR reactions were performed by using primers for either the CNDP2 WT allele (Forward: 5'-CAGATGGCTCGGAGATACCAC-3', Reverse: 5'-TTCCCGCTCCACCAAGGTGAAG-3') or CNDP2 KO allele (Forward: 5'-GCTCTGTAAGGGAAAGAGATGACCC-3', Reverse: 5'-AATAGGACATACCCAGTTCTGTGAGG-3'). The Promega GoTaq master mix was used for the PCR reaction. Each 25 μl reaction consisted of 12.5 μl of the promega master mix (M7122), 2.5 μl of a 10 μM mixture of forward and reverse primers, 2 μl of genomic DNA, and 8 μl of ultrapure water. The thermocycling program on BioRad C1000 Touch Thermo Cycler began with an initial 30 seconds at 95°C, followed by cycles of 30 seconds at 98°C, 30 seconds at 58 °C, and 45 seconds at 72 °C, followed by 5 minutes at 72 °C and finally held at 4 °C. PCR reactions for WT primers consisted of 30 cycles while PCR reactions for KO primers consisted of 48 cycles. Samples were run on a 2% agarose gel with 0.2 mg/ml EtBr. WT alleles are expected to yield a PCR product 160 base pairs in size while KO alleles are expected to yield PCR products that are 440 base pairs in size.

Acute feeding and water intake assays

DIO mice were individually housed and allowed ad libitum access to high-fat diet pellets and water for 5 days before the start of the experiment. On the day of the experiment, high-fat diet pellets were replaced with fresh pellets. Mice were then injected with either vehicle or BHB-Phe (50 mg/kg, i.p.) and high-fat diet and water intake were measured after 18 h.

Indirect calorimetry

DIO mice were singly housed in metabolic chambers and allowed ad libitum access to high-fat diet pellets and water. Metabolic parameters including oxygen consumption, carbon dioxide production, RER, food intake and ambulatory movement of mice were measured using a CLAMS system (Columbus Instruments) at the Stanford Diabetes Research Center. Mice were housed in the metabolic chambers for 48 h prior to the start of experiment. Energy expenditure calculations were normalized for body weight.

Leptin, ghrelin and GDF-15 measurements

Plasma was collected from DIO mice 1 h after the administration of BHB-Phe (50 mg/kg, IP) or vehicle. ELISA kits for leptin (Crystal Chem 90030), ghrelin (Cayman Chemicals 10006307) and GDF-15 (R&D Systems DY6385-05) were used following manufacturer's instructions.

Effect of GLP-1R antagonism on BHB-Phe-induced suppression of feeding

DIO mice were singly housed and allowed ad libitum access to high fat diet pellets and water. GLP-1 and BHB-Phe were dissolved in 18:1:1 (by volume) of saline/Kolliphor EL (Sigma Aldrich)/DMSO and Exendin-3 was dissolved in saline. Exendin-3 was added into BHB-Phe or GLP-1 solutions and the combined solution was administered daily (5 μl/g body weight) by intraperitoneal injection (Exendin-3, 0.1 mg/kg/day; BHB-Phe 50 mg/kg/day; GLP- 1: 2 mg/kg/day). Food intake and body weight were measured every day.

Effect of GFRAL antagonism on BHB-Phe-induced suppression of feeding

DIO mice were singly housed and allowed ad libitum access to high fat diet pellets and water. Mice received subcutaneous injections of anti-GFRAL antibody or control IgG at 10 mg/kg (2.6 μl/g body weight) once every 3 days and intraperitoneal injections of BHB-Phe at 50 mg/kg or vehicle (5 μl/g body weight) every day. Food intake and body weight were measured every day.

Effect of GDF-15 on body weight and food intake in mice injected with anti-GFRAL antibody

DIO mice were singly housed and allowed ad libitum access to high-fat diet pellets and water. Mice were injected with GFRAL neutralizing antibody or control IgG (10 mg/kg) once every three days for chronic experiments. Then, GDF-15 was dissolved in saline and injected subcutaneously at 4 nmol/kg (1 μl/g body weight) and the effect on food intake and body weight was measured after 24 h.

Sequential TRAP/c-Fos mapping BHB-Phe- and Lac-Phe-activated neurons in the brain

4-hydroxytamoxifen (4-OHT) (Sigma, Cat# H6278) was dissolved at 20 mg/ml in ethanol by sonication at 37°C for 15 min. The dissolved 4-OHT was then stored in aliquots at -80°C for up to several weeks or used immediately. Before use, 4-OHT was dissolved by shaking at 37°C for 10 minutes, then sunflower seed oil and castor oil (4:1) was added for a final concentration of 10 mg/ml. After evaporating the ethanol in a vacuum (3000 rpm, 15 minutes), the final 4-OHT solution was injected intraperitoneally (i.p.) at 50 mg/kg. To TRAP BHB-Phe-activated neurons, TRAP2/Rosa26-LSL-tdTomato male mice received IP injection of BHB-Phe (50 mg/kg), followed by 4-OHT injection (50 mg/kg, i.p.) 30 min after; two weeks later, the same mice received Lac-Phe (50 mg/kg, i.p.) and were perfused with saline followed by 10% formalin 90 min after the injection. To TRAP Lac-Phe-activated neurons, a separate group of TRAP2/Rosa26-LSL-tdTomato male mice received intraperitoneal injection of Lac-Phe (50 mg/kg), followed by 4-OHT injection (50 mg/kg, i.p.) 30 min after; two weeks later, the same mice received BHB-Phe (50 mg/kg, i.p.) and were perfused 90 min after the injection. As controls, another group of TRAP2/Rosa26-LSL-tdTomato male mice received IP injection of vehicle, followed by 4-OHT injection (50 mg/kg, i.p.) 30 min after; two weeks later, the same mice received vehicle injection (i.p.) and were perfused 90 min after the injection. Coronal brain sections were cut at 30 μm and collected into five consecutive series. One series of the sections was blocked for 1 hour in 0.3% PBST with 5% normal donkey serum. To detect c-Fos expression, the Rabbit anti-c-fos antibody (1:1000, #2250, Cell Signaling Technology) was added and incubated at 4°C overnight on shaker. The following day, slices were rinsed with 0.1% PBST for 3 ×10 minutes and then incubated with donkey anti-rabbit AlexaFluor 488 (1:1000, A21206, Invitrogen) at room temperature for 2 hours. Sections were cover-slipped and analyzed using a fluorescence microscope. The numbers of tdTomato-labeled (TRAPed) neurons and c-Fos-labelled neurons were counted and quantified manually. Three mice were included in each group.

QUANTIFICATION AND STATISTICAL ANALYSIS

Statistical analysis was performed in Prism 10.2.3. All data was expressed as mean ± SEM unless otherwise specified. A student's two-sided t-test was used for pair-wise comparisons. Two-way ANOVA with repeated measures in one factor were used for time course data of repeated measurements. Unless otherwise specified, statistical significance was set as $P < 0.05$. The specific test, P value symbol and error bar meaning, definition of center, and number of replicates are noted in figure legends.

CellPress
OPEN ACCESS

Supplemental figures

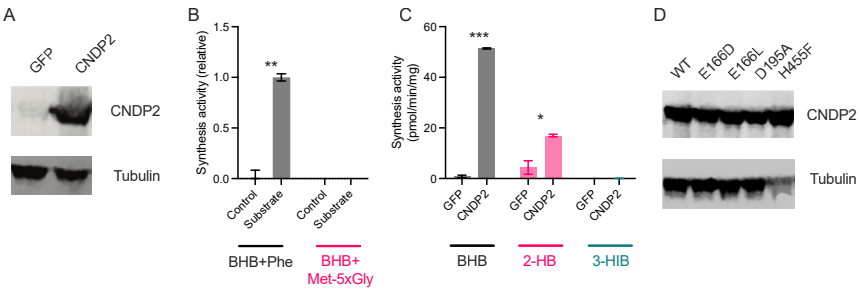

Figure S1. Additional *in vitro* characterization of CNDP2 activity, related to Figure 1

(A) Western blot using an anti-CNDP2 (top) or anti-tubulin (bottom) antibody for HEK293T cells transfected with either CNDP2-FLAG or GFP.

(B) Synthesis activity of recombinant purified mouse CNDP2-FLAG protein provided with the indicated substrates (10 mM each).

(C) Synthesis activity of GFP or mouse CNDP2-FLAG transfected HEK293T cell lysates that were provided with the indicated substrates (10 mM each).

(D) Western blotting using an anti-CNDP2 (top) or anti-tubulin (bottom) antibody for HEK293T cells transfected with either WT-CNDP2 or the indicated CNDP2 mutants.

For (B) and (C), reactions were performed at 37°C for 1 h.

For (B) and (C), n = 3–4/group. Data are shown as mean ± SEM. p values were calculated by Student's two-sided t test.

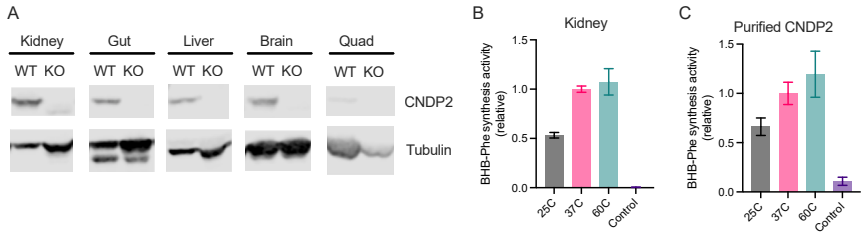

Figure S2. Additional characterization of tissue CNDP2 activity, related to Figure 2

(A) Western blot of WT or CNDP2-KO mouse tissues using an anti-CNDP2 (top) or anti-tubulin (bottom) antibody.

(B and C) Temperature dependence of BHB-Phe synthesis activity of kidney lysate (B) or recombinant purified mouse CNDP2-FLAG protein (C) in the presence of BHB and phenylalanine substrates at 20 mM.

For (B) and (C), reactions were performed at the indicated temperature for 1 h.

For (B) and (C), $n = 3$ per group. Data are shown as means ± SEM. p values were calculated by Student's two-sided t test.

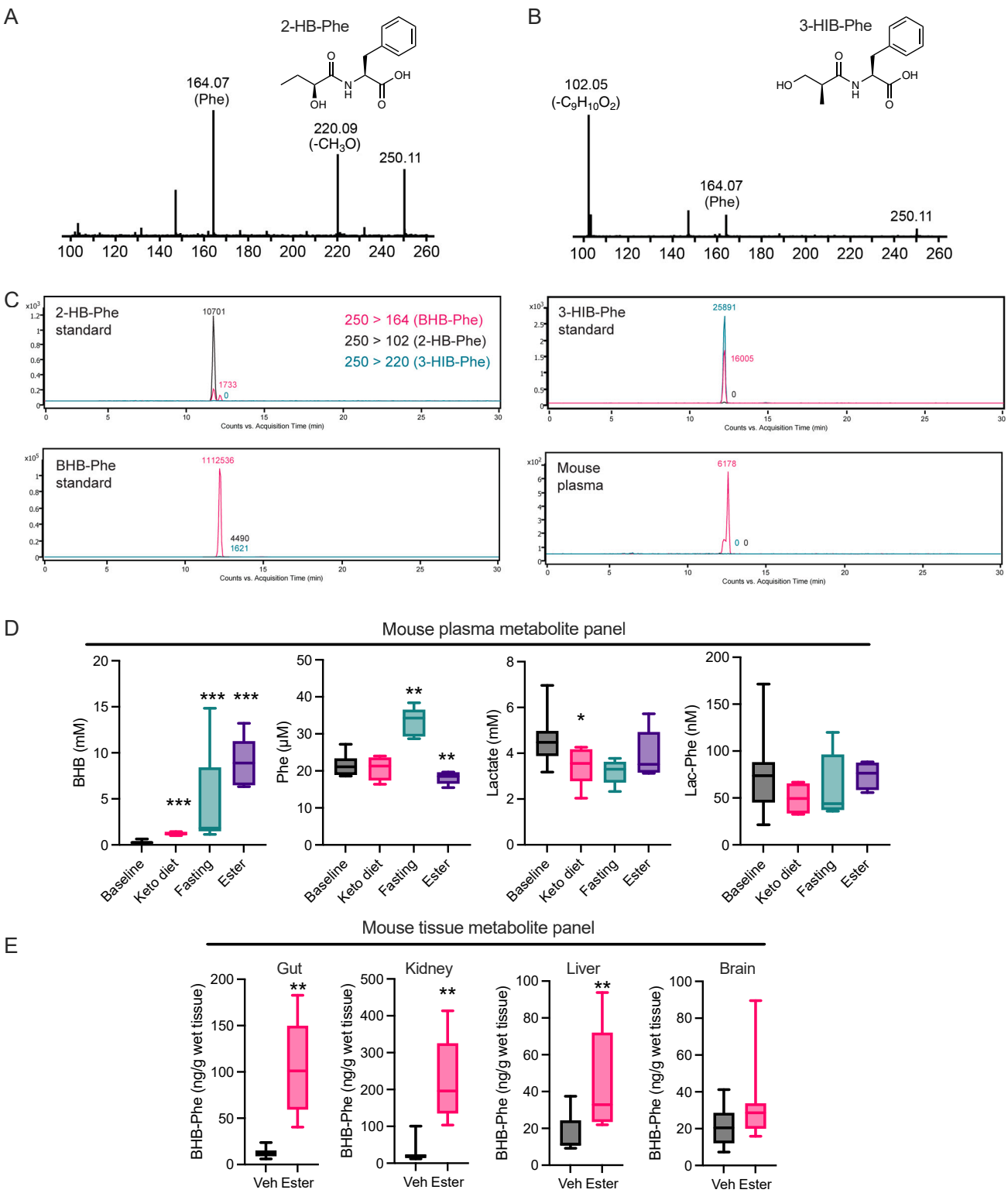

Figure S3. Additional characterization of mouse metabolites, related to Figure 3

(A and B) Structure (left) and tandem mass spectrometry fragmentation (right) for 2-HB-Phe (A) and 3-HIB-Phe (B).

(C) Relative abundances for the indicated MRM transitions for the indicated sample (authentic BHB-Phe, authentic 2-HB-Phe, authentic 3-HIB-Phe, or mouse plasma).

(legend continued on next page)

(D) BHB, phenylalanine, lactate, and Lac-Phe quantitation in 8- to 9-week-old male C57BL/6J mouse plasma at baseline, after 1 week on a ketogenic diet (Research Diets D21021803), after a 24-h fast, or 30 min post ketone monoester drink administration by oral gavage (3 g KE/kg of body weight).
(E) BHB-Phe quantitation in gut, kidney, liver, and brain from 18-week-old DIO mice 60 min post vehicle or ketone monoester drink administration (3 g KE/kg of body weight) by oral gavage.
For (D), $n = 5$ per group, with the baseline $n = 15$ (pooled from each of the three groups). For (E), $n = 7$ per group. Data are shown as box-and-whisker plots. p values were calculated by Student's two-sided t test.

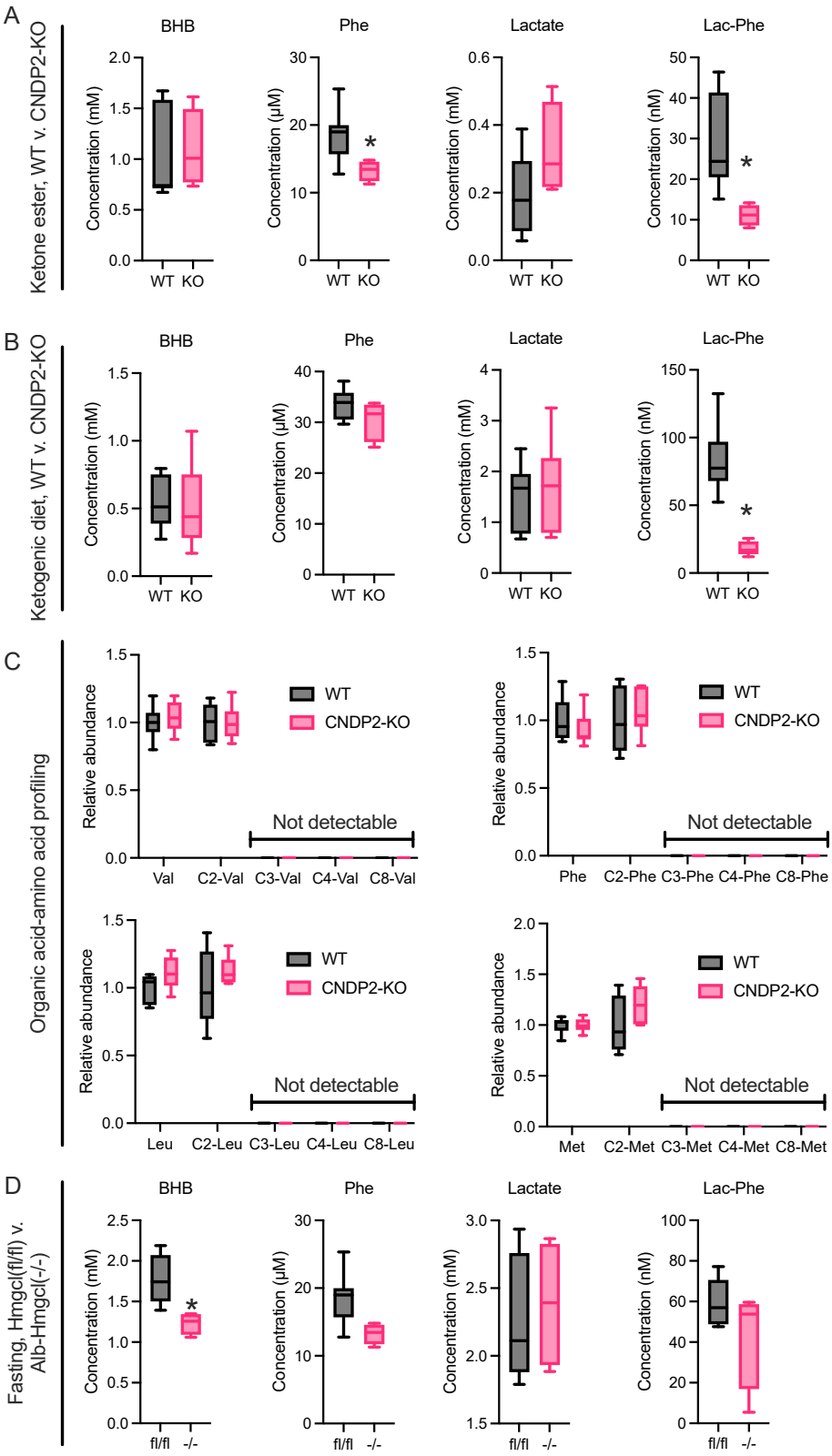

(legend on next page)

Figure S4. Additional characterization of mouse metabolites in the genetic models, related to Figure 4

(A) Quantitation of the indicated metabolites in plasma from 4- to 10-week-old male WT and CNDP2-KO mice at 60 min post ketone monoester drink administration (3 g KE/kg of body weight) by oral gavage.

(B) Quantitation of the indicated metabolites in plasma from 7- to 16-week-old female WT and CNDP2-KO mice after 1 week on a ketogenic diet (Research Diets D06040601).

(C) Quantitation of the indicated monocarboxylate-amino acid conjugates in plasma from 4- to 10-week-old female WT and CNDP2-KO mice.

(D) Quantitation of the indicated metabolite in plasma from Hmgcl (fl/fl) vs. Alb-Hmgcl($-/-$) mice after a 24-h fast.

For (A), $n = 7$ for WT and $n = 4$ for KO. For (B), $n = 10$ per group. For (C), $n = 6$ per group. For (D), $n = 5$ for *Hmgcl*$^{fl/fl}$, $n = 4$ for *Alb-Hmgcl*$^{-/-}$. Data are shown as box-and-whisker plots. p values were calculated by Student's two-sided t test.

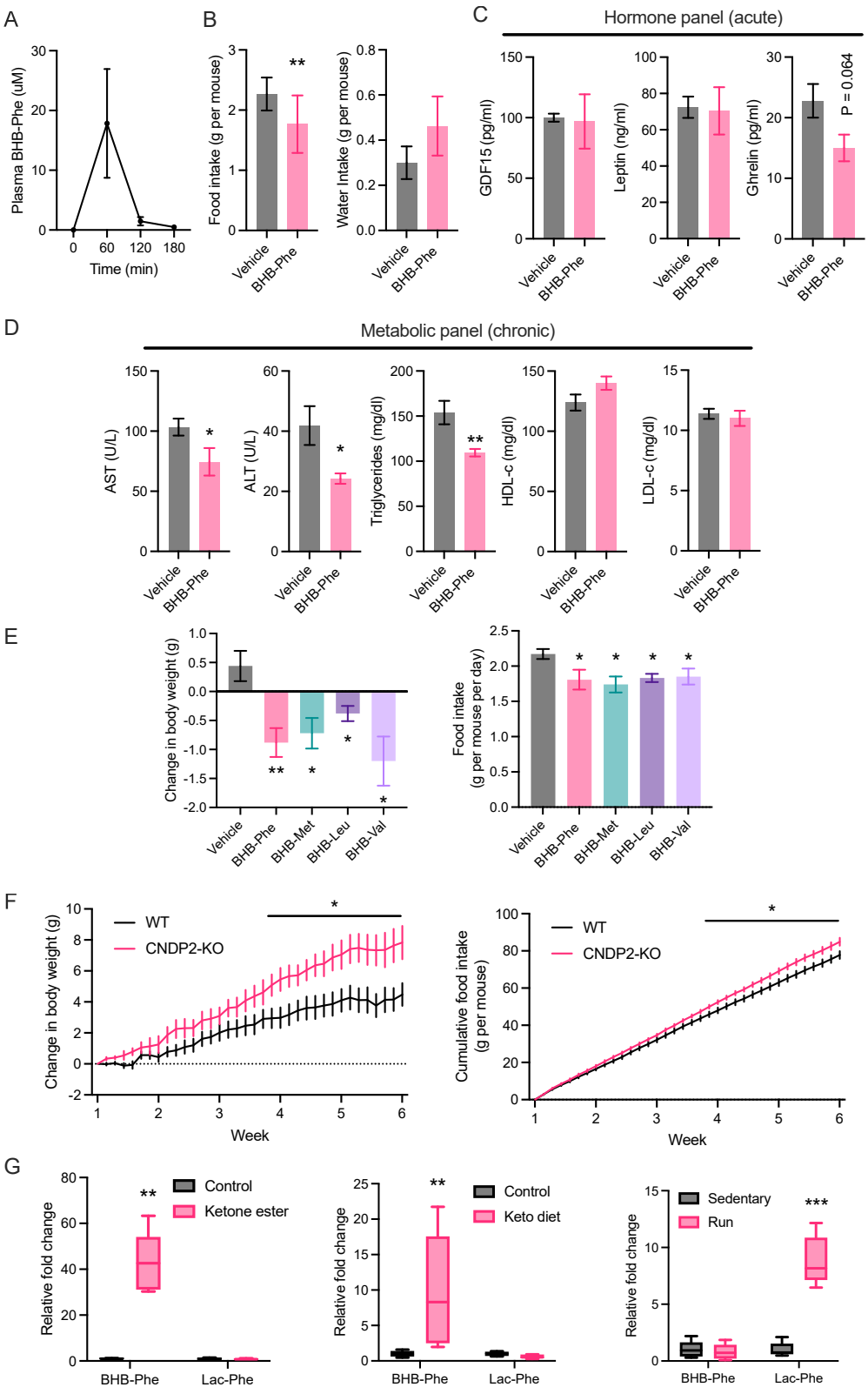

(legend on next page)

Figure S5. Additional metabolic characterization of mice treated with BHB-Phe and CNDP2-KO mice, related to Figure 5

(A) Plasma levels of BHB-Phe in 14-week-old male DIO mice following a single injection of BHB-Phe (50 mg/kg, i.p.).

(B) Food intake (left) and water intake (right) of 16-week-old male DIO mice following a single injection of vehicle or BHB-Phe (50 mg/kg, i.p.).

(C) Plasma acyl-ghrelin, leptin, and GDF15 plasma levels of 18-week-old male DIO mice 1 h after a single injection of vehicle or BHB-Phe (50 mg/kg, i.p.).

(D) Plasma AST ALT, TG, HDL-c, and LDL-c after 14 days of treatment with vehicle or BHB-Phe (50 mg/kg, i.p.).

(E) Change in body weight (left) and food intake (right) of 15-week-old male DIO mice after 5 days of treatment with vehicle, BHB-Phe, BHB-Leu, BHB-Val, or BHB-Met (50 mg/kg/day, i.p.). Starting body weights were vehicle: 38.6 ± 1.7 g, BHB-Phe: 38.6 ± 1.6 g, BHB-Met: 40.3 ± 1.7 g, BHB-Leu: 43.0 ± 1.9, BHB-Val 38.3 ± 1.5 g (mean ± SEM).

(F) Change in body weight (left) and food intake (right) of 14- to 18-week-old male WT and CNDP2-KO mice under a ketogenic diet (Research Diets D06040601) over a period of 6 weeks. Starting body weights were WT: 30.2 ± 0.8 g, CNDP2-KO: 30.6 ± 1.0, $p > 0.05$ (mean ± SEM).

(G) Relative fold change in BHB-Phe or Lac-Phe levels in the indicated comparison.

For (A), $n = 5$ per group. For (B), $n = 9$ per group. For (C), $n = 5$ for vehicle and $n = 4$ for BHB-Phe. For (D), $n = 8$ per group. For (E), $n = 5$ per group. For (F), $n = 9$ for WT and $n = 6$ for CNDP2-KO mice. For (G), $n = 5$ per group. For (A)–(F), data are shown as the mean ± SEM. For (G), data are shown as box-and-whisker plots. p values were calculated by Student's two-sided t test or two-way ANOVA.

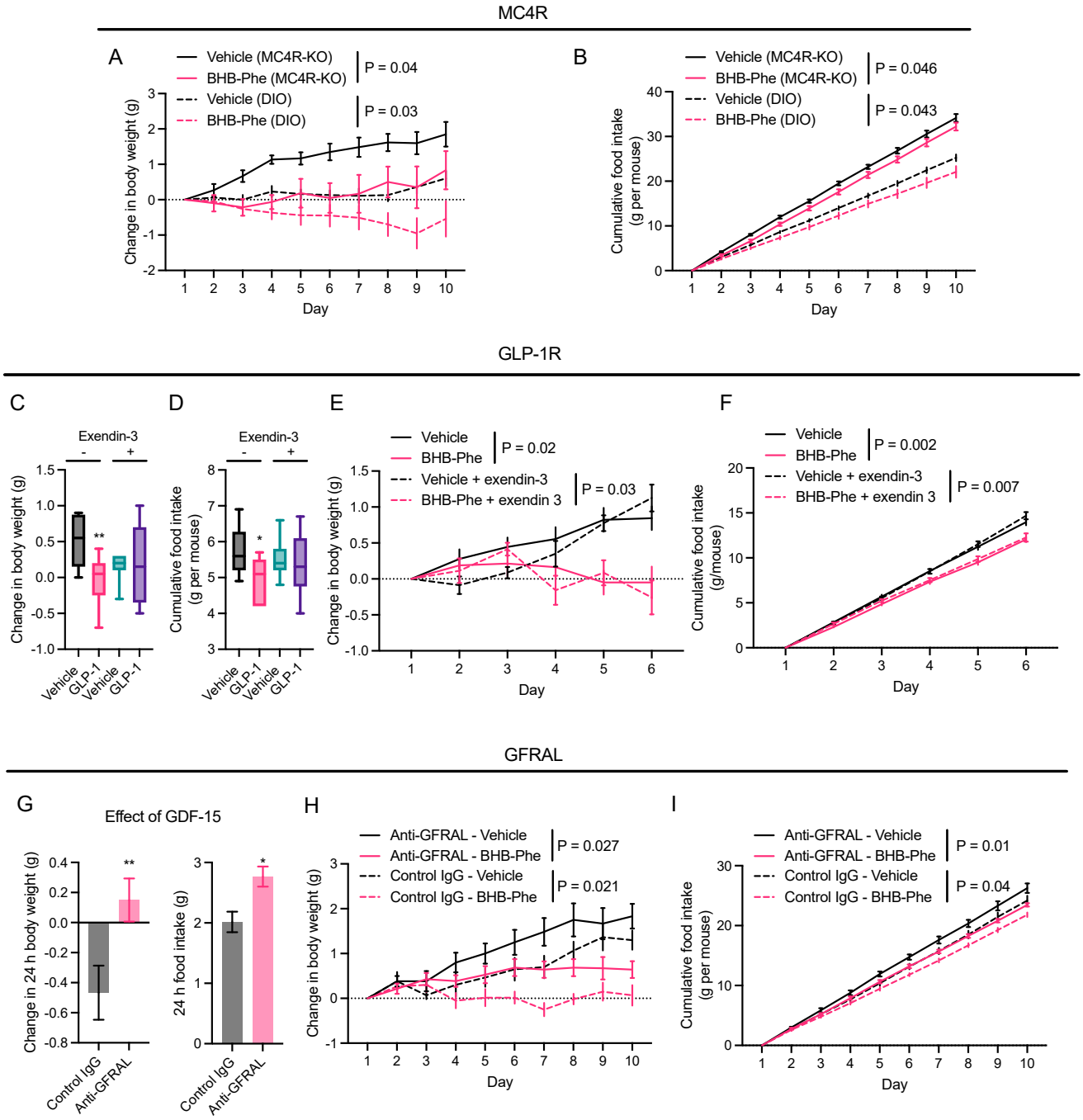

Figure S6. Role of MC4R, GLP-1R, and GFRAL pathways in the anorexigenic effects of BHB-Phe, related to Figure 6

(A and B) Change in body weight (A) and food intake (B) of 17- to 20-week-old male MC4R-KO mice on HFD or 17-week-old male DIO mice after treatment with vehicle or BHB-Phe (50 mg/kg/day, i.p.) or vehicle. Starting body weights were MC4R-KO/vehicle: 55.7 ± 1.9 g, MC4R-KO/BHB-Phe: 55.7 ± 1.7 g, MC4R-KO, DIO/vehicle: 42.8 ± 1.0 g, DIO/BHB-Phe: 41.9 ± 0.7 g (mean ± SEM).

(C and D) Change in body weight (C) and food intake (D) of 16- to 19-week-old male DIO mice after 3 days of treatment with vehicle or GLP-1 (2 mg/kg/day, i.p.) alone or with Exendin-3 (0.1 mg/kg/day, i.p.) co-treatment.

(E and F) Change in body weight (E) and food intake (F) of 16- to 19-week-old male DIO mice after 5 days of treatment with vehicle or BHB-Phe (50 mg/kg/day, i.p.) alone or with Exendin-3 (0.1 mg/kg/day, i.p.) co-treatment. Starting body weights were vehicle: 39.6 ± 1.3 g, BHB-Phe: 40.3 ± 1.5 g, vehicle/Exendin-3: 40.0 ± 1.4 g, BHB-Phe/Exendin-3: 40.7 ± 1.4 g (mean ± SEM).

(G) Effect of a single dose of GDF15 (4 nmol/kg, SQ) on body weight (left) and food intake (right) on 21-week-old male DIO mice in the presence of anti-GFRAL antibody (10 mg/kg, SQ) or IgG control antibody (10 mg/kg, SQ).

(legend continued on next page)

(H and I) Change in body weight (H) and food intake (I) of 20-week-old male DIO mice after 9 days of treatment with vehicle or BHB-Phe (50 mg/kg/day, i.p.) or vehicle in the presence of anti-GFRAL antibody (10 mg/kg, SQ) or IgG control antibody (10 mg/kg, SQ). Starting body weights were IgG/vehicle: 43.6 ± 1.8 g, IgG/BHB-Phe: 43.7 ± 1.3 g, anti-GFRAL/vehicle: 43.7 ± 1.3, anti-GFRAL/BHB-Phe 43.4 ± 2.2 g (mean ± SEM).

For (A) and (B), $n = 10$ per group for DIO and $n = 6$ per group for MC4R-KO. For (C)–(F), $n = 8$ per group. For (G), $n = 5$ per group. For (H) and (I), $n = 6$ per group. Data are shown as the mean ± SEM or as box-and-whisker plots. p values were calculated by Student's two-sided t test or by two-way ANOVA.

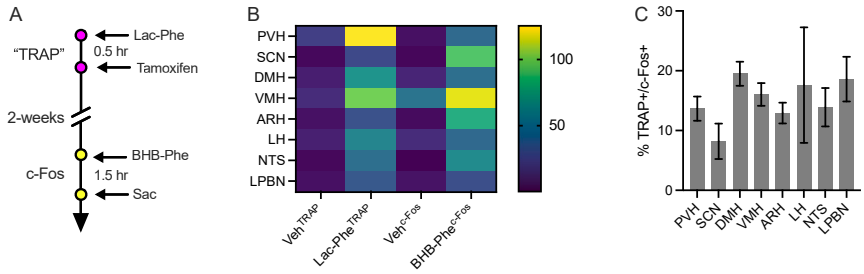

Figure S7. Additional characterization of TRAP/c-Fos mapping BHB-Phe- and Lac-Phe-activated neurons in the brain, related to Figure 6

(A) A schematic diagram illustrating the "reversed" TRAP experimental design. TRAP, targeted recombination in active populations.

(B) Heatmap showing the number of Veh^{TRAP}-, $Lac\text{-}Phe^{TRAP}$-, $Veh^{c\text{-}Fos}$-, and $BHB\text{-}Phe^{c\text{-}Fos}$-labeled neurons in various brain regions. ARH, arcuate nucleus of the hypothalamus; DMH, dorsomedial hypothalamus; LH, lateral hypothalamus; LPBN, lateral parabrachial nucleus; NTS, nucleus of the solitary tract; PVH, paraventricular hypothalamus; SCN, suprachiasmatic nucleus; VMH, ventromedial hypothalamus.

(C) Quantification of double-positive TRAP+/c-Fos+ neurons in the indicated brain regions.

For (B) and (C), $n = 3$ per group. Data are shown as mean ± SEM.